Self-Similar Magnetocentrifugal Disk Winds with Cylindrical Asymptotics

Eve C. Ostriker
Harvard-Smithsonian Center for Astrophysics, 60 Garden St., Cambridge, MA 02138
and
Department of Astronomy
University of Maryland, College Park MD 20742; ostriker@astro.umd.edu (present address)

ABSTRACT

We construct a two-parameter family of models for self-collimated, magnetized outflows from accretion disks. As in previous magnetocentrifugal wind solutions, a flow at zero initial poloidal speed leaves the surface of a disk in Kepler rotation about a central star, and is accelerated and redirected toward the pole by rotating, helical magnetic fields which thread the disk. At large distances from the disk, the flow streamlines asymptote to wrap around the surfaces of nested cylinders, with velocity $\mathbf{v}$ and magnetic field $\mathbf{B}$ directed in the axial ($\hat{z}$) and toroidal ($\hat{\varphi}$) directions. In the asymptotic regime, the velocity secularly decreases with cylindrical radius R from the inside to the outside of the flow because successive streamlines originate in the circumstellar disk in successively shallower portions of the stellar potential. In contrast to previous disk wind modeling, we have explicitly implemented the cylindrical asymptotic boundary condition to examine the consequences for flow dynamics. The present solutions are developed within the context of r-self-similar flows, such that $\mathbf{v}$, the density ρ, and $\mathbf{B}$ scale with spherical radius r as $\mathbf{v} \propto r^{-1/2}$, $\rho \propto r^{-q}$, and $\mathbf{B} \propto r^{-(1+q)/2}$; q must be smaller that unity in order to achieve cylindrical collimation. We self-consistently obtain the shapes of magnetic field lines and the θ-dependence of all flow quantities. The solutions are characterized by q together with the ratios $R_{\rm A}/R_1$ and R_0/R_1, where for a given streamline R_0 is the radius of its footpoint in the disk, $R_{\rm A}$ is the cylindrical radius where the flow makes an Alfvén transition, and R_1 is its final asymptotic cylindrical radius. For given q and R_0/R_1, $R_{\rm A}/R_1$ must be found as an eigenvalue such that the Alfvén transition is made smoothly. In the solutions we have found, the asymptotic poloidal speed v_z on any streamline is typically just a few tenths of the Kepler speed ΩR_0 at the corresponding disk footpoint, while the asymptotic rotation speed v_φ may be a few tenths to several tenths of ΩR_0. The asymptotic toroidal Alfvén speed $v_{{\rm A},\varphi} = B_\varphi/\sqrt{4\pi\rho}$ is, however, a few times ΩR_0; thus the outflows remain magnetically dominated, never making a fast-MHD transition. We discuss the implications of these models for interpretations of observed optical jets and molecular outflows from young stellar systems. We suggest that the difficulty of achieving strong collimation in vector velocity simultaneously with a final speed comparable to ΩR_0 argues against isolated jets and in favor of models with broader winds.

1. Introduction

1.1. Observational Context

Energetic, collimated jets and outflows are produced by accreting systems in a wide range of astronomical environments, from young stars forming in cold molecular gas clouds, to white dwarfs, neutron stars, and black holes in evolved binaries, to supermassive black holes within active galactic nuclei (e.g. Livio (1997)). Radiation pressure, thermal pressure, and magnetic stresses may all play a role in accelerating and collimating such flows. For the case of low-mass pre-main-sequence (PMS) stars, the high mass and momentum losses observed (Lada (1985),Edwards, Ray, & Mundt (1993), Fukui et al (1993), Bachiller (1996)) have led theorists to believe that magnetic forces are the essential ingredient in driving these winds (e.g. Königl & Ruden (1993), Shu (1996)). The densities and velocities involved place such flows from young stars in the regime of nonrelativistic magnetohydrodynamics (MHD). The prevalence of jets and outflows from pre-main-sequence stars argues that they are an inevitable byproduct of star formation; outflows may in fact help determine the eventual mass of the star that forms (Shu, Adams, & Lizano (1987)), and also have a profound influence on the dynamical evolution of the parent cloud (Norman & Silk (1980)). Thus, understanding the physics of cold, nonrelativistic MHD winds from accreting systems is crucial for modeling of star formation, and also informative for studies of other systems where magnetic fields are probably important in driving and confining winds – but where electromagnetic, thermal, radiative, and relativistic effects may complicate the dynamics (e.g. Begelman, Blandford, & Rees (1984), Blandford (1990)).

A topic of great theoretical and observational interest in studies of PMS stars is the dynamical connection between the fast, ionized jets seen near the presumed polar axis of the wind, and the slower and less-collimated molecular outflows that surround them. Molecular outflows are sometimes "jetlike" in appearance (Bachiller & Gomez-Gonzalez (1992)) but often more poorly confined spatially, while still having strongly directed bipolar momenta (e.g. Lada & Fich (1996)). Large outflow masses and red/blue lobe asymmetries argue that the bulk of the material in molecular outflows is swept up from the surrounding cloud rather than itself comprising a wind, but there is still no definitive model for the process that imparts momentum to the cloud. The observed line-of-sight-velocity/plane-of-sky-position distributions of outflow material must reflect the combined distributions of density in the ambient medium and forces or momentum fluxes that drive the molecular flow. Hence, although mass and momentum maps and line profiles from outflows are not directly invertible to yield the full outflow density distribution $\rho(\mathbf{v}, \mathbf{x})$, they can be used to help discriminate among different proposals for the nature of the primary wind and outflow acceleration mechanism (e.g. Masson & Chernin (1992), Chernin & Masson (1995), Nagar

et al (1997)). Models in which the outflow consists of a shell of ambient matter swept up by a wide-angle radial primary wind in a momentum-conserving fashion appear able to account for many observed outflow properties, provided appropriate stratification exists in both wind and ambient media (Shu et al (1991), Li & Shu (1996)). In alternative models, the primary wind is assumed to be jetlike (axial flow velocities) and the molecular outflow is the manifestation of a bow shock in the ambient medium (e.g. Blondin, Fryxell, & Königl (1990), Masson & Chernin (1993), Raga & Cabrit (1993), Stone & Norman (1993),Chernin et al (1994)). In this case the component of the outflow momentum transverse to the jet is driven by pressure gradient forces in the working surfaces at the jet head and within the jet (when variability leads to internal shocks), and the agreement with observed outflow properties depends very sensitively on the cooling rate of shocked gas.

The present uncertainty about outflow acceleration mechanisms highlights (and derives from) a more basic uncertainty regarding the origin and nature of the primary wind which is ultimately responsible for both the observed jets and outflows. Because observed velocities of optical jets are comparable to stellar escape speeds, the jet material almost certainly originates near the star. Jets appear quite collimated in density down to distances within a few tens of AU of the source (Ray et al (1996)). The observed optical jets are likely only the ionized, strongly-emitting inner portions of a broader, neutral wind with lower density and lower outflow speed than the jet (for observational evidence, see e. g. Heathcote et al (1996), Hartigan (1997) and references therein). The presence of separate high and low velocity blueshifted components in forbidden line profiles suggests that these winds may originate over a range of radii in the circumstellar disks (Hartigan, Edwards, & Ghandour (1995)). An open question, however, is whether the apparent collimation of optical jets is due to cylindrical *density* stratification of a primarily radial MHD wind which originates near the star (Shu et al (1995), Li (1996b)), or whether there is an MHD wind originating in an extended region of the disk (out to ~ 100 AU) which is itself well-collimated in *both* velocity and density, and which helps to collimate the observed jet and drive the larger-scale outflow (e.g. Pudritz & Norman (1986), Königl & Ruden (1993)). If observations end up demanding the latter, many uncertainties remain in models for MHD disk winds, especially in relation to the requirements for producing a collimated (but not recollimated) flow without singularities or other unphysical behavior. In the remainder of this Introduction, we describe current ideas about MHD winds driven from rapidly-rotating accreting systems ("magnetocentrifugal winds"), and discuss some of the difficulties in previous models of disk winds. This motivates the present work, which develops models for magnetocentrifugal winds that are constrained to become fully collimated at large distances from the source, and describes the general properties of such flows.

1.2. Magnetocentrifugal Disk Winds

The basic physics of steady magnetocentrifugal winds has been outlined in numerous sources; for a recent pedagogical review, see Spruit (1996). Heyvaerts & Norman (1989) and Heyvaerts & Norman (1996) have used analytic arguments to predict how asymptotic streamline collimation should develop in winds with varying properties (an analogous treatment for the relativistic case is given by Chiueh, Li, & Begelman (1991)). The mixed hyperbolic and elliptic nature of the general governing equations (Heinemann & Olbert (1978)), however, leads to technical difficulties in formulating and finding exact solutions for the steady-state problem in terms of appropriate boundary conditions (see e.g. Bogovalov (1994)), due to the presence of critical surfaces – projected to curves in the poloidal plane – within the flow. Nevertheless, steady-state, fully two-dimensional solutions have been obtained for the specific cases of a "split-monopole" poloidal magnetic field interior boundary condition (Sakurai (1985), Sakurai (1987)), and for the case of an "X-point" poloidal magnetic field interior boundary condition – strongly pinched magnetic fields fanning out of the disk near the star (Shu et al (1994b), Najita & Shu (1994), Shu et al (1995)).

To circumvent the difficulties associated with free critical surfaces, an approach that was earlier adopted by Blandford & Payne (1982) (hereafter BP) is to look for families of solutions with certain pre-determined symmetries. In BP, the fundamental assumption is that all velocities obey the same $v \propto r^{-1/2}$ scaling with spherical radius as the Kepler velocity, and that the density obeys $\rho \propto r^{-3/2}$ (the scaling associated with a mass-conservative spherical wind radially flowing in a Kepler potential). The magnetic field components then must behave as $B \propto r^{-5/4}$ in order to have the corresponding Alfvén speed $v_{\rm A}^2 = B^2/(4\pi\rho) \propto r^{-1}$. By assuming these scalings for the radial dependence of all quantities, the governing PDEs of the MHD wind problem are converted to ODEs in angular coordinate θ (or, as many workers have framed the problem, in the scaled height above the midplane). The assumed similarity scaling results in any critical surface coinciding with a radial line ($\theta = const.$). Blandford & Payne (1982) obtained a family of solutions which successfully navigated the Alfvén transition, directly demonstrating that cold MHD winds from rotating disks can reach large velocities and collimate their streamlines toward the poles.

The BP r-self-similar solutions have subsequently been extended and generalized by other workers, including relativistic solutions by Li, Chiueh, & Begelman (1992) and Contopoulos (1994), and nonrelativistic solutions with different basic scalings by Contopoulos & Lovelace (1994) (hereafter CL) and Ferriera (1996). In addition, Sauty & Tsinganos (1994) and Trussoni, Sauty, & Tsinganos (1996) have obtained MHD wind

solutions with different basic symmetry (latitudinal, rather than radial, self-similarity) via alternative choices for separation of variables, for application to flows from rapidly-rotating stars rather than accretion disks.

Eventually, a theory of magnetocentrifugally driven winds should be able to treat time-dependent, non-axisymmetric configurations with a fully self-consistent connection to the disk or star where the flow originates, and to the surrounding medium. Time-dependent, axisymmetric simulations of outflows from accretion disks have begun to be pursued by, e.g. Uchida & Shibata (1985), Shibata & Uchida (1986), and Stone & Norman (1994) (who include the internal disk dynamics), and by Ustyugova et al (1995), Koldoba et al (1995), and Ouyed, Pudritz, & Stone (1997) (who treat the disk as a boundary condition for the wind). The simulations produced so far verify that well-collimated MHD outflows (sometimes with intriguing time variability) can be generated by differentially-rotating disks threaded by a mean magnetic field, and that rapid disk accretion can occur as a result of angular momentum removal by the wind. However, the major technical effort required to produce these simulations (as well as the steady fully-2D solutions cited above) makes it difficult to explore parameter space extensively. Thus, it remains quite useful to study the properties of magnetocentrifugally driven outflows with models that impose a symmetry in advance to reduce the problem to coupled ODEs. The r-self-similar ansatz may be particularly appropriate for modeling outflows from accretion disks with a large dynamic range of radii, in which the flow may approach a scale-free solution well away from the boundaries. Indeed, the simulations of Ouyed, Pudritz, & Stone (1997) demonstrate that steady, r-self-similar winds may naturally develop when a mass flux is driven from the surface of a magnetized, rotating disk.

1.3. Wind-Driven Accretion

In general, accretion in a disk may be driven in part by local stresses (acting on radial scales comparable to the disk thickness, and often parameterized by an "α" viscosity, e.g. Pringle (1981)), and in part by larger-scale forces such as those associated with global spiral density waves (e.g. Spruit (1987)) or an MHD disk wind (e.g. BP, Pudritz & Norman (1986)). An interesting special case of an accretion disk/wind system is the extreme one where the disk wind from a given annulus removes the angular momentum and energy needed for what is left of the disk to accrete to the next annulus closer to the star. If we assume a steady state for both wind and disk, the conservation equations yield a differential

mass transfer rate $|d\dot{M}_W/dR| = |d\dot{M}_D/dR|$ at radius R, with

$$\frac{d\ln \dot{M}_W}{d\ln R}\left(\frac{J}{\Omega R^2}-1\right)=\frac{1}{2}, \tag{1}$$

in terms of the specific angular momentum J in the wind and the local Kepler rotation rate of the disk Ω (this expression assumes a thin disk in Kepler rotation). For self-similar solutions where density $\rho \propto r^{-q}$ in both the wind and disk, this would imply that the wind requires a ratio of the cylindrical Alfvén radius $R_{\rm A}$ to the streamline footpoint radius R_0 of

$$\frac{R_{\rm A}}{R_0}=\left(\frac{4-2q}{3-2q}\right)^{1/2} \tag{2}$$

because $J = \Omega R_{\rm A}^2$ (see §2.1). Solutions which lose very little mass in the outer disk (q nearly 3/2) must carry large specific angular momentum, and conversely, solutions with massive winds from their outer disks (small q) must have relatively low specific angular momenta in their winds if they are to be consistent with a steady state inflow/outflow.

Even if the Alfvén radius does not satisfy equation (2), a self-similar MHD disk wind will drive inflow in the disk with the disk accretion rate $\dot{M}_D(R)$ a power-law in R. For these more general cases, the surface density at any point in the disk would either increase or decrease in time depending on whether $R_{\rm A}/R_0$ is greater or less than the value in equation (2); the local mass deposition/removal timescale would be greater than the local accretion timescale by a factor $2\left[3-2q-1/((R_{\rm A}/R_0)^2-1)\right]^{-1}$.

The connection between mass and angular momentum loss in the wind and accretion in the disk was explored by Königl (1989) and Wardle & Königl (1993), using local models for the disk and connecting to the BP wind solutions; they showed that the field geometry required for a disk wind can be self-consistently provided by a diffusive (ambipolar or Ohmic) disk. The work of Li (1995) and Ferreira & Pelletier (1995) incorporating additional dynamics supported these conclusions. Most recently, Ferriera (1996) has obtained steady, r-self-similar combined inflow/outflow solutions for the case of ordinary resistivity in the disk region, while Li (1996a) has obtained steady inflow/outflow solutions assuming ambipolar diffusion in the disk (although neither set of solutions treats the wind far from the disk in a complete fashion; see below). In both of the last two cases, the solutions have $q > 1.4$, corresponding to a relatively small fraction of the disk mass being lost to a wind.

1.4. Critical Points and Wind Asymptotics

An outflow that accelerates from low velocity near the surface of an accretion disk to high velocities at a distance (permitting escape from the gravitational potential) may

pass through several points where the flow changes physical character. Such transitions occur when the flow speed surpasses the speed of an allowed wave mode (sound waves for unmagnetized or MHD waves for magnetized winds), and are manifest by apparent singularities in the equations governing the flow. Accounts of the nature of critical points in general and restricted MHD winds are given, e. g., by Heinemann & Olbert (1978), Spruit (1996), Tsinganos et al (1996); we summarize some of the main points here.

An important issue is whether, and where, the equations pass from being elliptic to hyperbolic at large distances from the source. Fully two-dimensional (axisymmetric) MHD flows become hyperbolic when the poloidal speed $v_{\rm p}$ exceeds the fast-mode MHD wave speed in the the poloidal direction $v_{\rm f} = (1/2)\left\{c_{\rm s}^2 + v_{\rm A}^2 + \left[(c_{\rm s}^2 + v_{\rm A}^2)^2 - 4c_{\rm s}^2 v_{\rm A,p}^2\right]^{1/2}\right\}$ (where $c_{\rm s}$ is the sound speed, $v_{\rm A}$ is the Alfvén speed, and $v_{\rm A,p}$ is the Alfvén speed associated with the poloidal magnetic field component $B_{\rm p}$). For a cold flow where $v_{\rm f} \to v_{\rm A}$, the fast-mode Mach number for the poloidal flow is $M_{\rm F} \equiv v_{\rm p}/v_{\rm A}$; the 2D equations become hyperbolic when $M_{\rm F} > 1$. The full 2D equations also have an apparent singularity at the Alfvén critical point where $v_{\rm p}/v_{\rm A,p} \equiv M_{\rm A} = 1$; here the fluid speed in the poloidal direction equals the wave speed of the Alfvén mode propagating in the poloidal direction.

As first pointed out by BP and recently reexamined in detail by Tsinganos et al (1996), the restriction to an r-self-similar model alters the nature of the critical points. With the assumption of r-self-similarity, the poloidal-plane PDE for cross-field force balance is converted to a second-order ODE in θ. Critical points in the equations now occur when the coefficient of the highest-order θ-derivative in the cross-field equation passes through zero. The modified fast-MHD and Alfvén points occur in the r-similar MHD equations, respectively, if $|v_\theta|/v_{f,\,\theta} = 1$ (where $v_{f,\,\theta}$ is obtained by replacing $v_{{\rm A},\theta}$ for $v_{\rm A,p}$ in the above expression for $v_{\rm f}$), and if $|v_\theta|/v_{{\rm A},\theta} = 1$. For a cold flow, $v_{\rm f} = v_{f,\,\theta} = v_{\rm A}$; the fast-MHD wave speed is the same for all propagation directions. For an r-similar flow the modified fast-MHD critical point would occur at $M_{\rm F}(|v_\theta|/v_{\rm p}) = |v_\theta|/v_{\rm A} = 1$, beyond the point $M_{\rm F} = v_{\rm p}/v_{\rm A} = 1$ where the fast-mode transition occurs (there are now no singularities in the equations at the location where $M_{\rm F} = 1$). Because $|v_\theta|/v_{{\rm A},\theta} = |v_{\rm p}|/v_{\rm A,p}$, the Alfvén point in the r-similar flow still occurs at $M_{\rm A} = 1$.

Physically, the modification of critical points happens because r-self-similar model flows remain *a priori* in effective causal contact in the $\hat{r}$ direction (as well as in the $\hat{\varphi}$ direction for assumed axisymmetric flows) for arbitrary Mach number. Thus critical transitions respect just the projection of the velocity in the direction of the spatial degree of freedom, $\hat{\theta}$, relative to the propagation speeds of the various wave families. In particular, effective "ellipticity" in the r-self-similar reduced equations is maintained as long as the $\hat{\theta}$ component of the velocity is smaller than the fast-MHD wave propagation speed in the $\hat{\theta}$ direction,

$v_{f,\theta}$ (= $v_{\rm A}$ for a cold flow). Geometrically, the condition is that the r-similar flow becomes effectively "hyperbolic" when the projection of the "minus characteristic" in the $\hat{\theta}$ direction becomes negative (cf. Tsinganos et al (1996); Contopoulos (1995)). The corresponding 2D equations remain *formally* hyperbolic (in the sense that characteristic curves are defined) in the whole region of the poloidal plane where $M_{\rm F} > 1$. Since, however, only the $\hat{\theta}$ direction is a spatial degree of freedom, only the projections of the characteristics in the $\hat{\theta}$ direction are relevant for the propagation of information from the boundaries into the body of the solution. Thus only if the flow were to pass through and remain at $|v_\theta|/v_{\rm A} > 1$ could we regard the information about the nature of boundary conditions at the pole as irrelevant to the solution. Even if such a solution were found, its relevance to real winds would be questionable because the propagation of information from the boundaries in the radial direction is ignored a priori.

More generally, full specification of the steady magnetocentrifugal wind problem requires both the flow equations and a statement of the desired boundary conditions. Whether or not the flow becomes hyperbolic, the interface with the ambient medium inside and outside the first and last streamlines of the outflow must, at least in principle, govern the latitudinal extent of a steady state wind (e. g. Shu et al (1995)). Since, however, the r-self-similar model is infinite radially – with infinite flux – there is no proper interior or exterior to the wind. The only solution boundaries for a cold, r-similar wind lie along $\theta = 0$ and $\theta = \pi/2$. The boundary at $\theta = \pi/2$ corresponds to the disk surface, where the solution should be able to match to a subsonic flow; several authors have discussed the additional constraints this imposes (see §1.3).

The boundary at $\theta = 0$ corresponds to the asymptotic limit of the flow at a large distance from the source. Even if an r-self-similar solution covers all angles, hence formally filling space and leaving no room for an ambient medium to match, a solution should be "physically reasonable" in the sense that if spatially truncated, the solution could be embedded within a larger (non-self-similar) solution without any very particular requirements. Thus, we would like to obtain self-similar solutions where the $\theta \to 0$ asymptotics could sensibly be matched to an ambient medium with generic properties. Such a matching would select among possible input parameters those which yield acceptable asymptotic solutions.

Previous r-similar MHD wind solutions containing both toroidal and poloidal fields – for a variety of scaling parameters – have not explicitly implemented matching to boundary conditions at the pole. In some work, numerically-integrated solutions are halted when they become singular near the modified fast-MHD point at $|v_\theta|/v_{\rm A} = 1$, since no regularity condition is applied (e.g. Ferriera (1996)). Other solutions are numerically integrated

away from the equator and halted at an arbitrary point near the pole, with $|v_\theta|/v_{\rm A} < 1$ throughout the computed region (e. g. BP and CL). A difficulty with these solutions is that many implicitly require special boundary conditions. Namely, a large class of solutions (with $q > 1$) generically recollimates (i.e. the cylindrical radius R of a streamline reaches a maximum and turns around), and another large class of solutions (with $q < 1$) generically shows radial oscillations of the streamlines (CL; see also Sauty & Tsinganos (1994)). Contopoulos & Lovelace (1994) found a third class of solutions (with $q > 1$) which does not show recollimation within the numerically-integrated regime, but they do not explicitly implement a $\theta \to 0$ asymptotic boundary condition.

On the other hand, Contopoulos (1995) has found a related solution with purely toroidal fields (where the flow does not accelerate from zero speed at the disk but instead requires a large initial poloidal injection speed, and since $v_{\rm A,p} \equiv 0$ there is never an Alfvén transition) with the input parameters tuned such that the solution makes a transition through the modified fast-MHD point $|v_\theta|/v_{\rm A} = 1$. While solutions containing both toroidal and poloidal fields can in principle make a transition through $|v_\theta|/v_{\rm A} = 1$, examples of such solutions have not yet been obtained due to the additional numerical effort demanded. The added requirement of making the $|v_\theta|/v_{\rm A} = 1$ transition would lower the number of free parameters in the solution by one, so that, for example, the two-parameter family of cold wind solutions of BP would become a one-parameter family.

In the present work, we set out find MHD wind solutions which *do* match to a specific asymptotic prescription. Inspired by observations which show strong collimation in both ρ and $\mathbf{v}$, we seek self-similar solutions which have cylindrical asymptotics. Thus, while our basic set of dynamical equations is equivalent to the cold wind equations of CL or Ferriera (1996) (although mathematically represented quite differently), we supplement them with an additional boundary condition at the pole ($\theta = 0$). The solutions we find are not global, in the sense that they do not directly connect onto the interstellar medium, or to the medium interior to the outflow (e.g. hot plasma, axial fields, or a mass-carrying MHD wind originating from the central object/inner disk). Nevertheless, the uniform cylindrical asymptotic behavior of these solutions allows a conceptual matching onto simple boundary conditions of constant (high) pressure interior, and (low) pressure exterior, to the region of the outflow. The levels of the ambient pressure would then select among the possible solutions by matching pressures at the boundaries. Although the condition of exactly cylindrical asymptotic collimation is probably more extreme than most real jet/outflows, the properties of these solutions makes clear the stark contrast in behavior between collimated and uncollimated magnetized flows.

1.5. Plan of Paper

In §2, we first (§2.1) state the governing equations for a steady, axisymmetric, MHD flow, then (§2.2) present an exact analytic solution for self-similar, differentially-rotating cylindrical flows which represent the chosen asymptotic boundary conditions far from the disk, and finally (§2.3) detail the r-similar wind *ansatz* and the resulting reduced forms of the wind equations. §3 presents solutions for disk winds that satisfy the self-similar equations with cylindrical asymptotics, and §4 discusses the properties of these solutions and compares to previous models and observations. Various mathematical details are described in appendices §§A.1-A.4

2. Magnetocentrifugal wind equations

2.1. Steady, axisymmetric ideal MHD equations

Consider a steady, axisymmetric magnetized flow with negligible resistivity. From axisymmetry, the poloidal magnetic field can be expressed in terms of a flux function Φ as

$$\mathbf{B}_p = \frac{-\hat{\varphi} \times \nabla\Phi}{R}, \tag{3}$$

where $R = r\sin\theta$ is the cylindrical radius. From the $\hat{z}$ component of the induction equation $\nabla \times (\mathbf{v} \times \mathbf{B}) = 0$, it can be shown that Φ is conserved on streamlines, $\mathbf{v}_p \cdot \nabla\Phi = 0$, and that

$$\mathbf{B}_p = \beta\rho\mathbf{v}_p \tag{4}$$

for some β – i.e. the poloidal streamlines and fieldlines are parallel. Combining the continuity equation $\nabla \cdot (\rho\mathbf{v}) = 0$ and $\nabla \cdot \mathbf{B} = 0$ shows that β, which represents the ratio of magnetic field to mass flux, is also conserved on streamlines: $\beta = \beta(\Phi)$ and $\mathbf{v}_p \cdot \nabla\beta = 0$. Defining

$$\Omega \equiv [v_\varphi - B_\varphi/(\beta\rho)]/R \tag{5}$$

and

$$\mathbf{u} \equiv \mathbf{v} - \Omega R\hat{\varphi}, \tag{6}$$

we obtain $\mathbf{B} = \beta\rho\mathbf{u}$, i.e. the flow in a frame rotating at Ω is frozen to the local field line. Using $\mathbf{v} \times \mathbf{B} = \Omega\nabla\Phi$ and the induction equation, one can show that $\nabla\Omega \times \nabla\Phi = 0$, so that Ω is constant along field lines. Thus $\Omega(\Phi)$ is the rotation rate of a given field line, and on the field line labeled by Φ in the frame rotating at Ω, the flow and field are parallel, $\mathbf{u} \parallel \mathbf{B}$. Each field line, of course, can have a different rotation rate $\Omega(\Phi)$. From equation (6), $\mathbf{u}_p = \mathbf{v}_p$; we use the symbols interchangably.

The toroidal component of the momentum equation yields an additional conserved quantity along field lines, the specific angular momentum J associated with the combined matter flow and Poynting flux

$$J = J(\Phi) = R(v_\varphi - \frac{\beta B_\varphi}{4\pi}). \tag{7}$$

Using the definition (6), we write

$$J = \Omega R^2 + R u_\varphi (1 - M_{\rm A}^{-2}) \equiv \Omega R_{\rm A}^2, \tag{8}$$

where we use the definition for the Alfvén Mach number $M_{\rm A}$ of the flow

$$M_{\rm A}^2 \equiv \frac{v_{\rm p}^2}{v_{\rm A,p}} = \frac{v_{\rm p}^2}{B_{\rm p}^2/(4\pi\rho)} = \frac{4\pi}{\beta^2\rho}. \tag{9}$$

Note that $v_{\rm p}/v_{\rm A,p} = u_\varphi/v_{\rm A,\varphi} = |\mathbf{u}|/v_{\rm A} = M_{\rm A}$. The Alfvén radius $R = R_{\rm A}$ is the point where a flow makes a transition from $M_{\rm A} < 1$ near the disk to $M_{\rm A} > 1$ in the wind.

Taking the component of the momentum equation in the direction of $\mathbf{B}$ yields the Bernoulli equation, which states that

$$\mathcal{E} \equiv \frac{1}{2}|\mathbf{u}|^2 + \frac{\gamma}{\gamma-1}\frac{P}{\rho} + V_{\rm g} - \frac{1}{2}\Omega^2 R^2 \tag{10}$$

is constant on field lines, $\mathcal{E} = \mathcal{E}(\Phi)$. Here, we have assumed an ideal gas with ratio of specific heats γ, and throughout this work we shall assume the gravitational potential $V_{\rm g} = GM/r$ of a central point mass. In the absence of heating and cooling, the final conserved quantity on field lines is the specific entropy, such that $K \equiv P\rho^{-\gamma} = K(\Phi)$.

The final dynamical equation is obtained by taking the component of the momentum equation along $\nabla\Phi$. The resulting Grad-Shafranov equation describes force balance in the direction perpendicular to the poloidal field $\mathbf{B}_p$, and can be written

$$\nabla\cdot\left[(1-M_{\rm A}^2)\frac{\beta\nabla\Phi}{4\pi R^2}\right] = \frac{B_\varphi}{R}\frac{dJ}{d\Phi} - \beta\rho\frac{d\mathcal{E}}{d\Phi} + \frac{|\mathbf{B}|^2}{4\pi}\frac{d\beta}{d\Phi} - R\beta\rho v_\varphi\frac{d\Omega}{d\Phi} + \frac{\beta\rho^\gamma}{\gamma-1}\frac{dK}{d\Phi}. \tag{11}$$

In this work, we will find it convenient to express the various flow and field variables in terms of Φ and the conserved quantities β, J, Ω, $\mathcal{E}$, and K. The toroidal speed in the rotating frame is obtained from equation (8) as

$$u_\varphi = \frac{J/R - \Omega R}{1 - M_{\rm A}^{-2}}; \tag{12}$$

the inertial-frame toroidal speed is

$$v_\varphi = \frac{J/R - M_{\rm A}^{-2}\Omega R}{1 - M_{\rm A}^{-2}}. \tag{13}$$

The magnitude of the poloidal speed can be obtained from equation (10) as

$$|\mathbf{u}_p|^2 = 2\mathcal{E} - 2V_{\rm g} + \Omega^2 R^2 - \left(\frac{J/R - \Omega R}{1 - M_{\rm A}^{-2}}\right)^2 - 2\frac{\gamma}{\gamma - 1}\frac{P}{\rho}. \tag{14}$$

An alternative expression for the poloidal speed comes from the definition (3) together with $\mathbf{u}_p = \mathbf{B}_p/\beta\rho$. Equating the two expressions yields an equation for ρ. For the case of a cold flow with $P = 0$, ρ is the solution of a quartic equation in terms of Φ, $\nabla\Phi$, β, J, Ω, $\mathcal{E}$ and $r,\ \theta$.

2.2. Self-similar magnetized cylindrical flows

In this section, we consider the steady, ideal, axisymmetric MHD equations without gravity, and find a class of solutions representing rotating, cylindrically self-similar flows. In these solutions, the poloidal velocity is everywhere axial ($\mathbf{v}_p \parallel \hat{z}$), all speeds scale with cylindrical radius $R = r\sin\theta$ as $v \propto R^{-1/2}$, the density scales as $\rho \propto R^{-q}$, and all components of the magnetic field scale as $B \propto R^{-(1+q)/2}$. All flow variables are independent of z. The cylindrical solutions have identical similarity scaling in $\sin\theta$ to their similarity scaling in r. These cylindrical solutions define the *asymptotic* angular behavior for the radially self-similar disk outflows considered in this work, which satisfy the general r-self-similar equations to be presented in §2.3 (i. e. the same radial scaling as the asymptotic state but arbitrary scaling in θ). For simplicity, we specialize here to cold flows ($P = 0$), but the more general expressions are easily derived.

Starting from the above *ansatz* for scalings, any solution must have $\Phi \propto R^{\frac{3-q}{2}}$, $\Omega \propto R^{-3/2}$, $\beta \propto R^{q/2}$, $J \propto R^{1/2}$, and $\mathcal{E} \propto R^{-1}$. The Alfvén Mach number $M_{\rm A}$ is uniform throughout the flow. In order to normalize these power-law solutions, we choose a fiducial field line $\Phi = \Phi_1$ lying along $R = R_1$, and rotating at a rate $\Omega_1 = \Omega(\Phi_1)$. We define $j \equiv J/\Omega R^2$, $e \equiv -\mathcal{E}/(\Omega R)^2$, and $m \equiv M_{\rm A}^{-2} = \frac{\beta^2\rho}{4\pi}$, all of which quantities are independent of R. Then, normalizing all speeds by $\Omega R = \Omega_1 R_1 (R/R_1)^{-1/2}$, we have inertial-frame toroidal velocity

$$\frac{v_\varphi}{\Omega R} = \frac{j - m}{1 - m}, \tag{15}$$

rotating-frame toroidal velocity

$$\frac{u_\varphi}{\Omega R} = \frac{j - 1}{1 - m}, \tag{16}$$

poloidal speed $v_p = v_z$

$$\frac{|v_p|}{\Omega R} = \left[1 - 2e - \frac{(j-1)^2}{(1-m)^2}\right]^{1/2}, \tag{17}$$

and toroidal and poloidal Alfvén speeds

$$v_{\mathrm{A},\varphi} = m^{1/2} u_\varphi \tag{18}$$

and

$$v_{\mathrm{A,p}} = m^{1/2} v_{\mathrm{p}}. \tag{19}$$

For the cold, zero-gravity solutions, the Bernoulli equation (10) with the cylindrical *ansatz* reduces to

$$\frac{|\mathbf{u}|^2}{(\Omega R)^2} = 1 - 2e, \tag{20}$$

so that $v_A^2/(\Omega R)^2 = m(1-2e)$. The only remaining constraint on the flow is the Grad-Shafranov equation (11), which for our present assumption of a cylindrically-stratified flow is just the $\hat{R}$ component of the momentum equation,

$$0 = \frac{v_\varphi^2}{R} - \frac{1}{8\pi\rho R^2}\frac{d(R^2 B_\varphi^2)}{dR} - \frac{1}{8\pi\rho}\frac{d(B_p^2)}{dR}, \tag{21}$$

where we have dropped the thermal pressure term assuming a cold flow (i.e. c_{s} small compared to the flow and Alfvén speeds). Now employing the self-similar scaling for the magnetic field $|\mathbf{B}| \propto R^{-(1+q)/2}$, this reduces to

$$0 = v_\varphi^2 + \frac{q-1}{2} v_{\mathrm{A},\varphi}^2 + \frac{1+q}{2} v_{\mathrm{A,p}}^2. \tag{22}$$

Substituting in equation (22) for v_φ, $v_{\mathrm{A},\varphi}$, and v_{A} in terms of e, j, and m, we arrive at the quadratic equation

$$0 = m^2(1-2e)\frac{1+q}{2} + m\left[\frac{1-q}{2} + (1+q)e\right] - j^2. \tag{23}$$

The physical solution has

$$M_{\mathrm{A}}^2 \equiv m^{-1} = (2j^2)^{-1}\left\{\frac{1-q}{2} + (1+q)e + \left[\left(\frac{1-q}{2} + (1+q)e\right)^2 + 2j^2(1+q)(1-2e)\right]^{1/2}\right\}. \tag{24}$$

Thus, given q and the values of the angular momentum and Bernoulli parameters j and e, we obtain cylindrical solutions by substituting equation (24) in equations (15)-(19). The

fast-mode Mach number $M_{\rm F} \equiv |\mathbf{v}_p|/v_{\rm A}$ is also constant throughout the cylindrical flow, and is written

$$M_{\rm F}^2 = M_{\rm A}^2 \left[1 - \frac{1}{(1-2e)} \left(\frac{1-j}{1-m}\right)^2\right]. \tag{25}$$

When $1-q >> j,\ e$, an approximate solution to equations (15-25) is $v_\varphi/(\Omega R) \approx j$, $v_{\rm p}/(\Omega R) \approx (2j-2e)^{1/2}$, $v_{{\rm A},\varphi}/(\Omega R) \approx j[2/(1-q)]^{1/2}$, $v_{\rm A,p}/(\Omega R) \approx 2j(j-e)^{1/2}(1-q)^{-1/2}$, $M_{\rm A} \approx j^{-1}[(1-q)/2]^{1/2}$, and $M_{\rm F} \approx j^{-1}(1-q)^{1/2}(j-e)^{1/2}$.

These self-similar cylindrical solutions only exist for a limited range of parameters. In particular, the original Blandford-Payne scaling $\rho \propto r^{-3/2}$, $B \propto r^{-5/4}$ is not compatible with the self-similar cylindrical asymptotic solutions described here. In fact, equation (22) can only be satisfied only for $q < 1$, i.e. when the density and magnetic field profiles are less steep than R^{-1} (the same criterion also holds when thermal pressure is included). Physically, this is true because the tension associated with the toroidal field is the only inward force that can oppose the outward centrifugal force and outward (for $q > -1$) force associated with the magnetic (and thermal) pressure gradient. Only for $q < 1$ is the hoop stress large enough to enforce cylindrical collimation, and the closer q is to 1, the larger the collimation radius relative to the launch point. Notice that it is only the inclusion of a toroidal field $v_{{\rm A},\varphi} \neq 0$ that permits cylindrical solutions for flows in which the magnetic pressure decreases outwards. In cases where the magnetic pressure (i.e. the fluid energy density) increases outward ($q < -1$), both the poloidal and toroidal components of the field apply stresses that oppose the centrifugal force in equation (22), and collimation occurs at relatively small radii. However, we do not consider cases with $q < -1$ likely to be appropriate models for winds from extended accretion disks, so we do not consider them further herein.

The axial current carried by the self-similar cylindrical flow scales as $R^{\frac{1-q}{2}}$. Therefore, for $q < 1$ the current increases with the radial scale of the flow, and there is no singularity at the axis. The total mass, momentum, and energy per unit time carried by the flow within R scale as $\dot{M} \propto R^{3/2-q}$, $\dot{P} \propto R^{1-q}$, and $\dot{E} \propto R^{1/2-q}$. Thus the cylindrical solutions with $q < 1$ have mass and momentum flows dominated by the outer regions, and energy flow dominated by the interior (exterior) for $q > 1/2$ ($q < 1/2$).

A further constraint on the parameter space for which self-similar cylindrical solutions exist is that the solution of equation (17) be real. The boundary of parameter space is found by equating $|\mathbf{v}_p| = 0$ and using equation (24); solutions exist for

$$j \geq \frac{2e}{1+(1-2e)^{1/2}} \left[1 + \frac{4e}{(1-q)} \frac{1}{(1+(1-2e)^{1/2})\,(1-2e)^{1/2}}\right]. \tag{26}$$

All solutions must have $e < 1/2$.

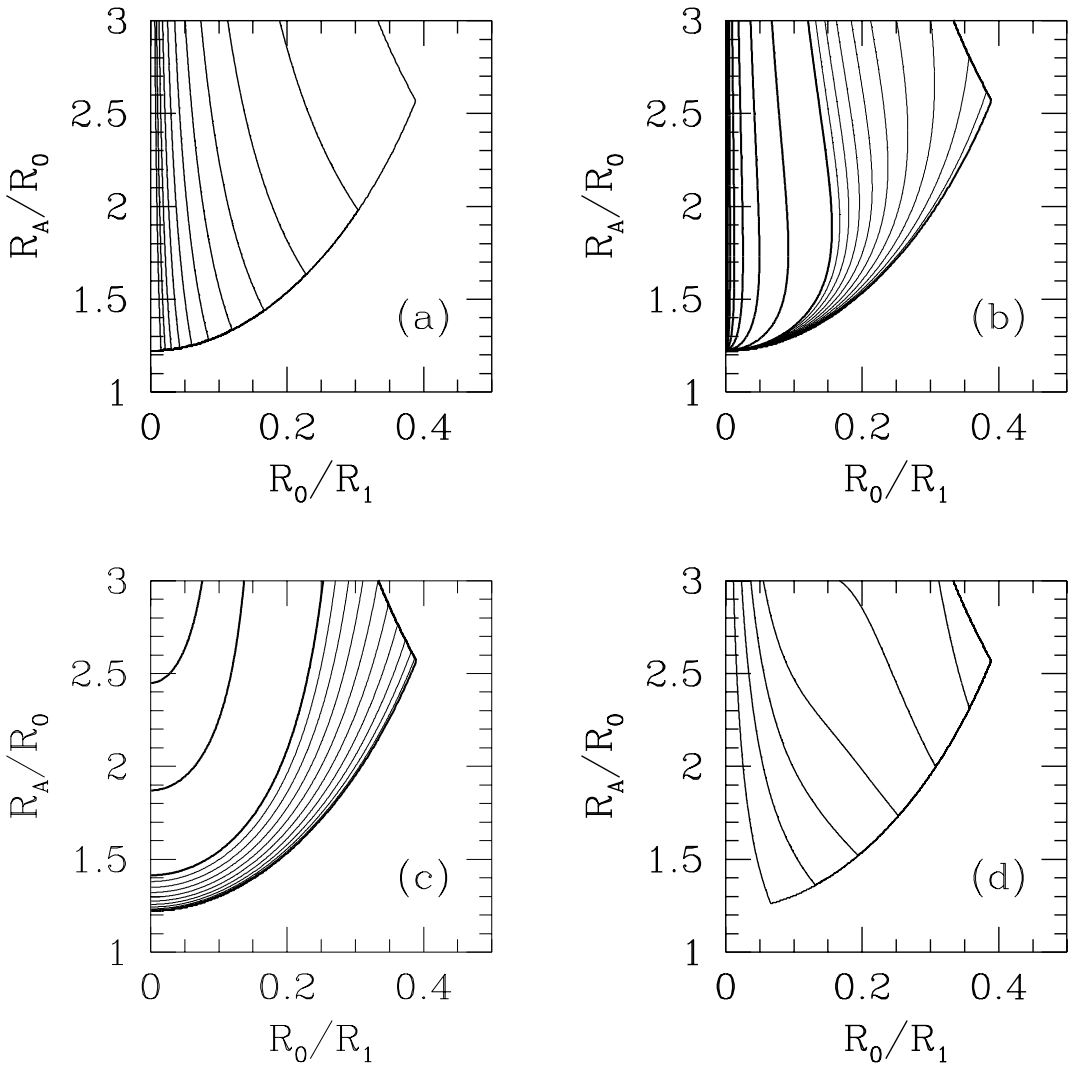

Fig. 1.— Parametric dependence on R_0/R_1 and R_A/R_0 of the asymptotic self-similar cylindrical solution family with $q = 0.75$. For a given cylindrical solution with field line rotation rate Ω, specific angular momentum J and Bernoulli constant $\mathcal{E}$ on the streamline through R_1, R_0 and R_A represent the cylindrical radii of the footpoint and Alfvén point a disk outflow would need in order to have the same $\Omega = \sqrt{GM/R_0^3}$, $J = \Omega R_A^2$, and $\mathcal{E} = -(3/2)(\Omega R_0)^2$. (a) Alfvén Mach number $M_A = v_p/v_{A,p}$. Contours show $M_A = 1, 2, 4, 8, ...$, from right to left. (b) Fast MHD Mach number $M_F = v_p/v_A$. Heavy contours show $M_F = 0, 1, 2, 4, 8, ...$ from right to left; light contours $M_F = 0.1, 0.2, 0.3, ...$ (c) Poloidal speed relative to Kepler speed on the disk. Heavy contours show $v_p/\Omega R_0 = 0, 1, 2, 3$, from right to left; light contours show $v_p/\Omega R_0 = 0.1, 0.2, 0.3, ...$ (d) Toroidal speed relative to Kepler speed on the disk. Contours show $v_\varphi/\Omega R_0 = 0.1, 0.2, 0.3, .., 0.6$ from left to right.

If we think of a given cylindrical solution as the asymptotic limit of an outflow from an accretion disk, we can express the parameters j and e in terms of important physical scales in the flow. From equation (8), $j = (R_{\rm A}/R_1)^2$, where $R_{\rm A}$ is the Alfvén radius for the streamline that asymptotes to R_1. From equation (10), the Bernoulli parameter is equal to its value where the flow leaves the disk. If the same cold flow streamline originates in a Keplerian disk at launch radius R_0, $\mathbf{u} = 0$ on the disk surface so $\mathcal{E} = -(3/2)(\Omega R_0)^2$. Using $\Omega^2 = GM/R_0^3$ for the fiducial streamline, $e = (3/2)(R_0/R_1)^2$. The flow speeds v_φ and v_z relative to the Kepler speed ΩR_0 at the footpoint of any streamline are found by multiplying the right-hand-sides of equations (15) and (17) by R_1/R_0. From equation (17), the ratio of the final speed to the Kepler speed at the launch point is bounded by

$$\frac{v_{\rm p}}{\Omega R_0} < \left[2\left(\frac{R_{\rm A}}{R_0}\right)^2 - 3\right]^{1/2}. \tag{27}$$

Figure 1 shows the dependence of $M_{\rm A}$, $M_{\rm F}$, v_φ, and v_p on the parameters $R_0/R_1 \equiv (2e/3)^{1/2}$ and $R_{\rm A}/R_0 \equiv [3j/(2e)]^{1/2}$ for an example of the cylindrical solution family with $q = 0.75$. At other values of q, the behavior is similar, with the right-hand "corner" of the solution moving toward smaller R_0/R_1 and larger $R_{\rm A}/R_0$ as q increases.

From equation (26), $j > e$ so a cold flow originating in a Kepler-rotating disk must have $(R_{\rm A}/R_0)^2 > 3/2$. Recalling from equation (2) that a fully self-similar inflow/outflow solution would have $(R_{\rm A}/R_0)^2 = (4-2q)/(3-2q)$, we note that this implies such solutions are only possible when $q > 1/2$. From equation (27), steady inflow/outflow solutions would need $v_{\rm p}/(\Omega R_0) < [(2q-1)/(3-2q)]^{1/2}$; since the maximum value of the right-hand side is one (for $q = 1$) the asymptotic axial wind speed for such solutions could not exceed the Kepler speed at the launch point ΩR_0.

2.3. Self-similar steady wind equations and nondimensionalization

Section 2.1 presents the general ideal MHD equations. Here, we specialize to the case of self-similar flows in which all the flow variables are power-laws in the spherical radius r, and in particular all velocities are required to follow the Kepler-law behavior $v \propto r^{-1/2}$. With this *ansatz*, we write the functional forms of the density, magnetic flux, field-line rotation rate, magnetic-to-mass flux ratio, total specific angular momentum, and Bernoulli parameter as

$$\rho \equiv \rho_1 \left(\frac{r\sin\theta}{R_1}\right)^{-q} n(\theta), \tag{28}$$

$$\Phi \equiv \Phi_1 \left(\frac{r\sin\theta}{R_1}\right)^{(3-q)/2} \phi(\theta), \tag{29}$$

$$\Omega \equiv \Omega_1 \left(\frac{r\sin\theta}{R_1}\right)^{-3/2} \omega(\theta), \tag{30}$$

$$\beta \equiv \beta_1 \left(\frac{r\sin\theta}{R_1}\right)^{q/2} b(\theta), \tag{31}$$

$$J \equiv J_1 \left(\frac{r\sin\theta}{R_1}\right)^{1/2} \ell(\theta), \tag{32}$$

and

$$\mathcal{E} \equiv \mathcal{E}_1 \left(\frac{r\sin\theta}{R_1}\right)^{-1} \epsilon(\theta). \tag{33}$$

In the above expressions, we have anticipated the asymptotic ($\theta \to 0$) functional form of the flow variables by explicitly including the appropriate power-law dependence in $\sin\theta$ in each definition. So that each quantity is normalized by its respective asymptotic value on $R = r\sin\theta = R_1$ (for $\theta \to 0$, $r \to \infty$,), we set $n(0) = 1$, $\phi(0) = 1$, $\omega(0) = 1$, $b(0) = 1$, $\ell(0) = 1$, and $\epsilon(0) = 1$. [1] As introduced in §2.2, we define the constants

$$m \equiv M_{\rm A}^{-2}|_{\theta\to 0} = \frac{\beta_1^2\rho_1}{4\pi}, \tag{34}$$

$$j \equiv \left.\frac{J}{\Omega R^2}\right|_{\theta\to 0} = \frac{J_1}{\Omega_1 R_1^2}, \tag{35}$$

and

$$e \equiv \left.\frac{-\mathcal{E}}{\Omega^2 R^2}\right|_{\theta\to 0} = \frac{-\mathcal{E}_1}{\Omega_1^2 R_1^2}; \tag{36}$$

for cold flow originating at R_0 in a Kepler-rotating disk, $j = (R_{\rm A}/R_1)^2$, $e = (3/2)(R_0/R_1)^2$, and m is given by equation (24). It is also convenient to define the constant

$$h \equiv \frac{v_{\rm p,1}^2}{(\Omega_1 R_1)^2} = 1 - 2e - \frac{(j-1)^2}{(1-m)^2} \tag{37}$$

[1] For a more general radially self-similar flow – not requiring cylindrical asymptotics – we could use the same form of the equations and instead normalize by fixing the values of n, ϕ, ω, etc. on an arbitrary $\theta = \theta_1$, $r = r_1$.

where $v_{\rm p,\,1}$ is the poloidal speed on the streamline asymptotic to R_1, and the final equality is derived from the asymptotic cylindrical solution (see eq. 17).

From §2.1, the functions Ω, β, J, and $\mathcal{E}$ are all field line invariants, such that $\Omega = \Omega_1$ on $\Phi = \Phi_1$, etc. From expressions (29) - (33), this implies that radially self-similar flows have

$$\omega = \phi^{-3/(3-q)},\ b = \phi^{q/(3-q)},\ \ell = \phi^{1/(3-q)},\ \text{and}\ \epsilon = \phi^{-2/(3-q)} \tag{38}$$

for all θ.

To derive an equation for the remaining flow function $n(\theta)$, we use the self-similar expressions (29) - (33) in the equations (3), (4), and (14) to obtain

$$\frac{hQ^2(\theta)}{(bn)^2} = 2\left(\frac{R_0}{R_1}\right)^3 \sin\theta - 2e\epsilon + \omega^2 - \left(\frac{j\ell - \omega}{1 - mnb^2}\right)^2 . \tag{39}$$

Here,

$$Q^2(\theta) \equiv \phi^2 \sin^2\theta + \left(\phi\cos\theta + \frac{2}{3-q}\phi' \sin\theta\right)^2 , \tag{40}$$

where we have set the field line rotation speed $\Omega_0 R_0$ at the footpoint R_0 equal to the Kepler speed $\sqrt{GM/R_0}$, and we drop the thermal energy term. Equation (39) is a quartic equation for $n(\theta)$ in terms of $\phi(\theta)$, $\phi'(\theta) \equiv d\phi/d\theta$, θ, and constant parameters.

To complete the set of wind equations, we must restate the Grad-Shafranov equation (11) in terms of the reduced self-similar functions defined in equations (29) - (33). The result is a (somewhat complicated) second-order O. D. E. which is linear in $\phi''(\theta)$; the full expression is given in §A.1 of the Appendix.

As described in §1.4, a self-consistent r-similar wind solution must either become effectively hyperbolic near the pole (with parameters tuned such that the corresponding critical transition through the modified fast MHD point is made smoothly), or else if it remains effectively elliptic, the solution must match some physically realistic boundary conditions at the pole (again, by appropriately tuning the input parameters). In the present work, we satisfy this requirement by matching explicitly to an analytic solution near the pole. We choose the R-similar cylindrical solution introduced in §2.2 as the $\theta = 0$ boundary condition for our r-self-similar solutions. As described earlier, this limits our choice of the scaling parameter to $q < 1$. Additional requirements on the asymptotic solution arising from this choice of polar boundary condition are described in §A.2.

For the cylindrical asymptotic solutions of this work, $M_{\rm A}$ and $M_{\rm F}$ become constant, and $|v_\theta|/v_p = \sin\theta$, which approaches zero near the pole – hence $|v_\theta|/v_{\rm A} \to 0$ near the pole, and solutions remain effectively elliptic. Furthermore, we have found that $M_{\rm F}$ remains < 1

throughout the flow for all the cylindrically-collimated solutions we obtain, so these models would be elliptic when considered as solutions of the full two-dimensional equations, as well. Thus, the solutions obtained in this work must negotiate only the first critical point, requiring a smooth transition through $M_{\rm A} = 1$. The conditions that must be met at the Alfvén point are detailed in §A.3.

The numerical solutions in this work are obtained by initiating the integrations at the pole, and tuning the input parameters until a smooth Alfvén transition is obtained. For some solutions, we find it convenient to match onto the sub-Alfvénic part of the flow with a numerical integration that starts at the equator; the two solutions then overlap in the sub-Alfvénic region. Once the input parameters have been found such that the flow integration initiated at the pole negotiates the Alfvén critical transition, such matching solutions require no additional choice of input parameters at the equator to be fully-specified. When using the shooting method and starting from the equator, however, it is necessary to search for the correct initial value of ϕ' at the equator such that a good match is obtained. The governing equations become singular at the equator for a cold flow (since $n \to \infty$ as $v \to 0$); the limiting behavior of the equations and implications for the equatorial boundary condition are discussed in §A.4.

3. Magnetocentrifugal disk wind solutions

In this section, we present solutions we have obtained for r-similar cold MHD flows that meet cylindrical (R-similar) boundary conditions at the pole. As explained in §§2.2-2.3, the solutions we obtain are described by q (the scaling parameter for which $\rho \propto r^{-q}$ and $B \propto r^{-(1+q)/2}$), and the two parameters $j = (R_{\rm A}/R_1)^2$ and $e = (3/2)(R_0/R_1)^2$, where R_0 is the radius of a streamline footpoint in the disk, $R_{\rm A}$ is the cylindrical Alfvén radius, and R_1 is the asymptotic cylindrical radius. For our numerical solutions, we fix q and R_0/R_1 and then vary $R_{\rm A}/R_0$ until the conditions for a smooth Alfvén transition are satisfied (see §A.3). We thus obtain a two-parameter family of solutions.

An example of a solution for $q = 0.75$ and $R_0/R_1 = 0.35$ is portrayed in Figure 2a-d. We find that the solution requires $R_{\rm A}/R_0 = 2.412438$ in order to make a smooth Alfvén transition; the Alfvén surface lies at $\theta = 18^\circ$ with respect to the pole. From Figures 2a and 2c, collimation becomes very rapid after the Alfvén transition has been made. From Figure 2c, it is apparent that there is no radial (R) oscillation of the streamlines; instead, in this and our other solutions the cylindrical radius R of any streamline secularly increases with height above the disk. From Figure 2b, notice that near the disk (at large θ) $v_{{\rm A},\varphi}$ rises above $v_{\rm A,p}$ even before the Alfvén transition is made. This effect occurs in all of the solutions

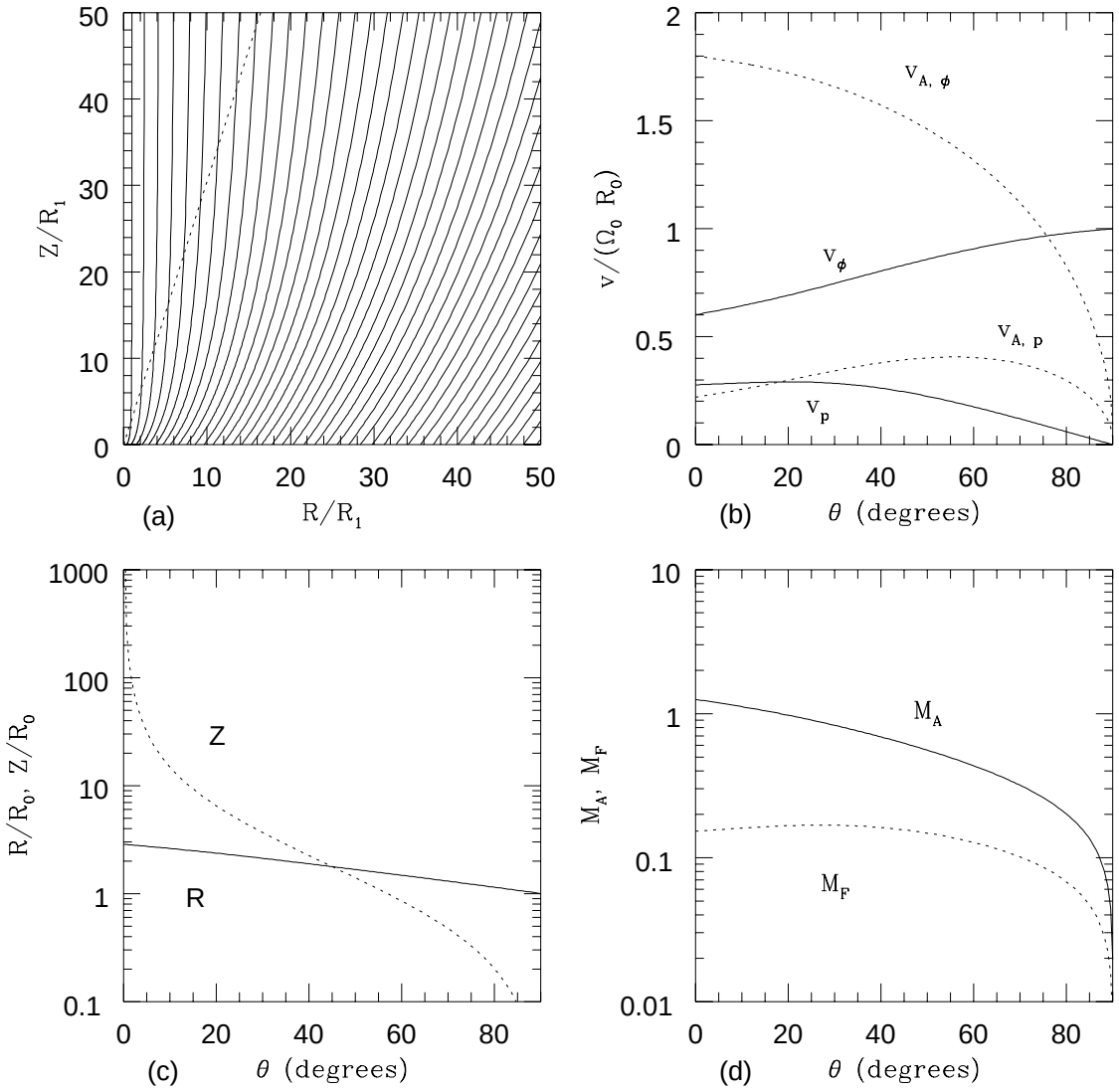

Fig. 2.— Flow solution for q=0.75, $R_0/R_1 = 0.35$, $R_A/R_0 = 2.41$. (a) Streamlines (solid curves) for equal increments in $\dot{M}$. The innermost streamline originates at $R/R_1 \equiv R_0/R_1 = 0.35$ on the abscissa and asymptotes to $R/R_1 = 1$ at infinite Z; the corresponding flow makes an Alfvén transition at $R/R_1 \equiv R_A/R_1 = 2.41$. The dashed line shows the locus of the Alfvén surface. (b) Fluid speeds (solid curves) and Alfvén speeds (dashed curves) of poloidal and toroidal flow/field components, in units of the Kepler speed $\Omega_0 R_0$ at the footpoint of a streamline, as a function of angle θ with respect to the pole. (c) Streamline radial distance (solid curve) and height above the disk (dashed curve) in units of the footpoint radius R_0 at the equator. (d) Alfvén-mode (solid curve) and fast-mode (dashed curve) Mach numbers for the flow, $M_A = v_p/v_{A,p}$ and $M_F = v_p/v_A$.

we have obtained. Thus, the acceleration in these flows may be thought of as largely due to the gradient in the toroidal field pressure, rather than primarily due to the centrifugal force in a rotating, nearly rigid, poloidal magnetosphere (cf. e.g. Spruit 1996). From Figure 2d, notice that the flow is sub-fast-MHD ($M_{\rm F} < 1$) throughout. This is also true for the rest of the solutions we have found. Another feature of Figure 2b which holds for the other flow solutions as well is that the asymptotic rotation speed exceeds the asymptotic poloidal (axial) speed. The slight decrease in poloidal speed $v_{\rm p}$ near the pole is also a general feature of our solutions.

While the general properties of the flow depicted in Fig. 2 is representative of all the solutions we have found, the quantitative characteristics of course differ for each solution. Figure 3a shows the relationship among the three parameters q, R_0/R_1, and $R_{\rm A}/R_0$ that characterise flows which become asymptotically cylindrical, for a number of solutions we have obtained which successfully make a smooth Alfvén transition. Numerically, $R_{\rm A}/R_0$ is obtained as an eigenvalue for any (q, R_0/R_1) pair. From Figure 3a, notice that the solutions all hug near the limiting locus ($v_{\rm p} = 0$) for cylindrical asymptotic solutions to exist. For fixed similarity scaling power q, solutions with relatively more angular momentum (large $R_{\rm A}/R_0$) collimate relatively close to their footpoints (large R_0/R_1), and also have their Alfvén radii relatively closer to the asymptotic cylindrical radius (large $R_{\rm A}/R_1$). For fixed ratio $R_{\rm A}/R_0$ of the Alfvén cylindrical radius to the streamline footpoint radius, an increase in the central concentration of the magnetic flux and density (i.e. an increase in q) implies a smaller value of R_0/R_1 – i.e. the solution expands to a larger cylindrical radius before collimating.

In Figure 3b, we show the corresponding value of $\theta_{\rm A}$, the angular distance of the Alfvén surface from the pole, for the solutions shown in Figure 3a. For fixed q, solutions which collimate relatively close to their footpoints (R_0/R_1 large) make their Alfvén transitions relatively near the pole ($\theta_{\rm A}$ small). For fixed R_0/R_1, the streamlines for different values of q follow very nearby paths, and the variation of the fluid speeds with angle θ is also quite similar for the solutions with differing q. On the other hand, the variation of the Alfvén speeds with θ differs significantly for solutions with different q and the same R_0/R_1; as q increases, the Alfvén speed at a given θ increases, thereby shifting the Alfvén point closer to the pole.

The asymptotic flow and Alfvén speeds vary with the flow parameters q, $R_{\rm A}/R_0$, and R_0/R_1. In Figure 4, we plot the values of these asymptotic speeds for the same set of solutions as in Figure 3. From Figure 4a, notice that for a given similarity scaling q, the asymptotic axial fluid speed increases as the Alfvén point moves further from the streamline footpoint ($R_{\rm A}/R_0$ increases). At fixed $R_{\rm A}/R_0$, solutions with increasingly concentrated

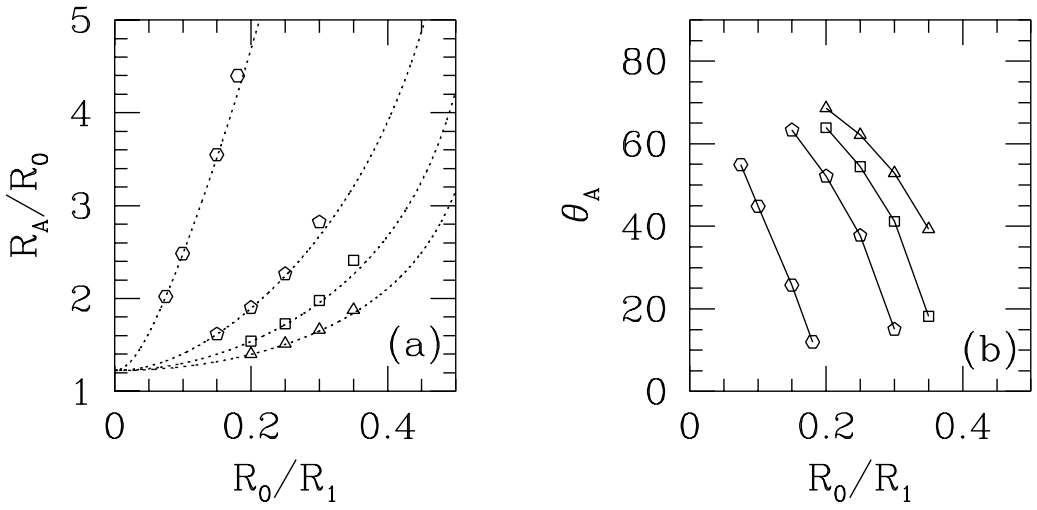

Fig. 3.— (a) Relation among parameters $R_{\rm A}/R_0$, R_0/R_1, and scaling power q, for several outflow solutions. R_0, $R_{\rm A}$, and R_1 are the respective cylindrical radii of the footpoint, Alfvén transition, and asymptotic lateral expansion of each streamline; $q = -\partial \log \rho / \partial \log r = -(1 + 2\partial \log B/\partial \log r)$. Triangles show solutions with $q = 0.5$; squares $q = 0.75$; pentagons $q = 0.9$; hexagons $q = 0.99$. The dashed curve shows the lower boundary for cylindrical asymptotic solutions to exist, i. e. the locus where $v_{\rm p} = 0$ for a self-similar cylindrical flow of given q (see eq. 26). (b) Angle of the locus of the Alfvén surface with respect to the pole, for the solutions in (a) (solid lines connect the solution points of given q).

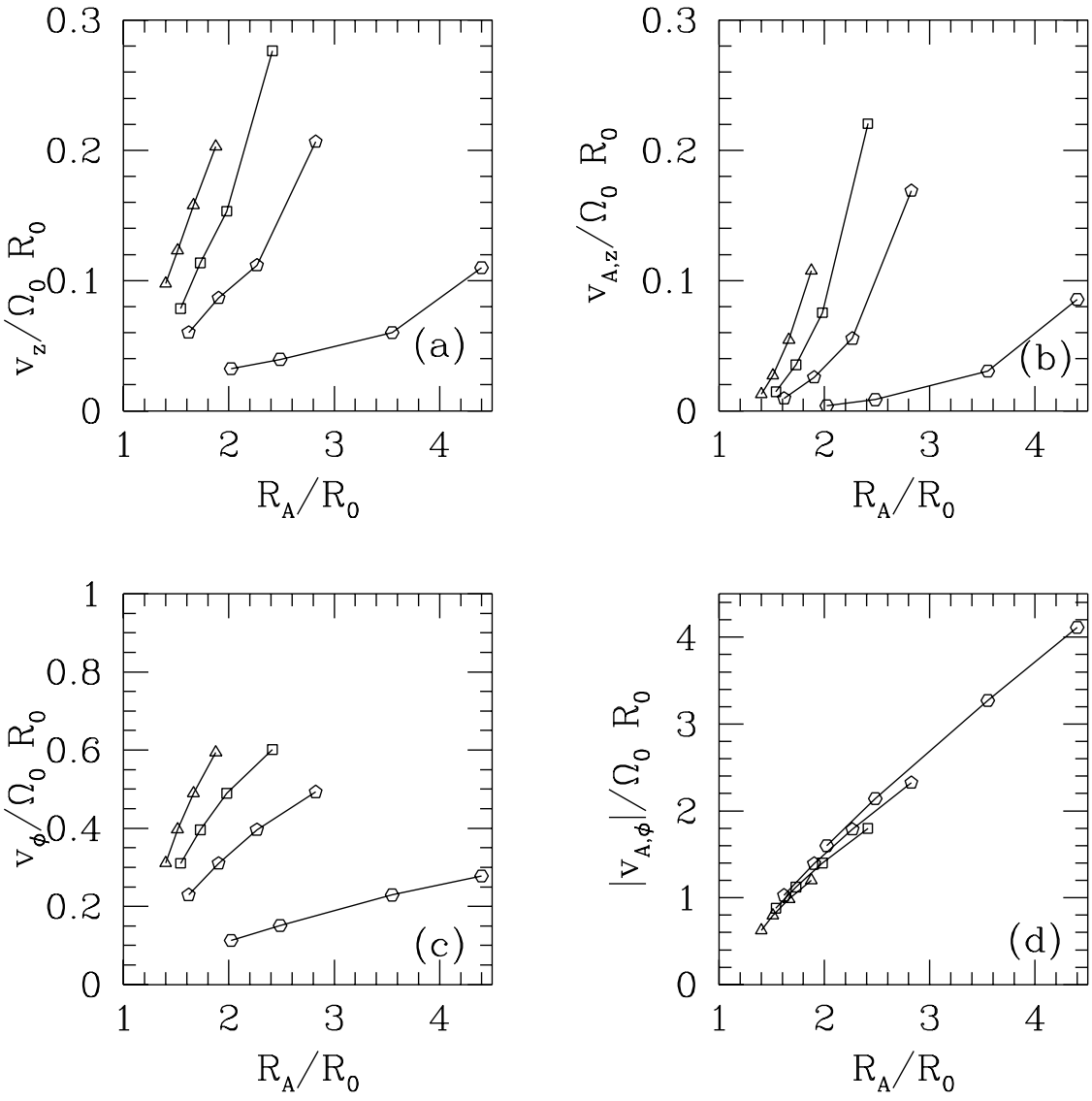

Fig. 4.— Asymptotic fluid and Alfvén speeds for full r-similar solutions with various parameters, in units of the Kepler speed at the streamline footpoint. Triangles show solutions with $q = 0.5$; squares $q = 0.75$; pentagons $q = 0.9$; hexagons $q = 0.99$. Solid lines connect the solution points. (a) Poloidal (axial) speed. (b) Poloidal Alfvén speed. (c) Toroidal speed. (d) Toroidal Alfvén speed.

magnetic flux (increasing q) have lower asymptotic v_z. From Figures 4b and 4c, the same trends hold for the poloidal Alfvén speed and the toroidal flow speed. Figure 4d shows that the asymptotic toroidal Alfvén speed increases with $R_{\rm A}/R_0$ for fixed q. At fixed $R_{\rm A}/R_0$, the toroidal Alfvén speed increases very slightly with the degree of flux concentration (increasing q). Note that none of the solutions displayed here have $R_{\rm A}/R_0$ sufficiently small to correspond to the case of a steady, self-similar inflow driven by the outflow at given q (cf. eq. 2). While we have identified some such solutions, the extremely low asymptotic poloidal speeds that they yield makes them unlikely candidates to model real outflows.

Figure 5a,b shows how the Alfvén and fast-MHD Mach numbers $M_{\rm A}$ and $M_{\rm F}$ for the asymptotic limit of the r-similar flow varies with the solution parameters. For fixed similarity scaling q, $M_{\rm A}$ decreases with increasing $R_{\rm A}/R_0$, while $M_{\rm F}$ slightly increases with $R_{\rm A}/R_0$. At fixed $R_{\rm A}/R_0$, an increase in the concentration of the flow (larger q) implies a larger asymptotic $M_{\rm A}$, but a smaller asymptotic $M_{\rm F}$. On the other hand, for fixed ratio of initial to final radius of a streamline R_0/R_1 (not shown), an increase in q implies both smaller $M_{\rm F}$ and $M_{\rm A}$, asymptotically.

The flow solutions we have obtained are in general magnetically dominated in the asymptotic regime, in the sense that for most of the solutions, the energy, momentum, and angular momentum fluxes of carried by Maxwell stresses exceed the respective kinetic fluxes. These flux ratios are given, respectively, by

$$\frac{E_K}{E_M} = \frac{|\mathbf{v}|^2 M_{\rm A}}{2\Omega R|v_{{\rm A},\varphi}|}, \tag{41}$$

$$\frac{P_K}{P_M} = (\frac{1}{2}M_{\rm F}^{-2} - M_{\rm A}^{-2})^{-1}, \tag{42}$$

and

$$\frac{J_K}{J_M} = \frac{v_\varphi M_{\rm A}}{|v_{{\rm A},\varphi}|}. \tag{43}$$

(Note that the small electric contribution $(1/2)M_{\rm A}^{-2}(\Omega R/c)^2$ to the denominator of equation (42) has been dropped.) Figure 6 shows the asymptotic values of these flux ratios for the same solutions as discussed above. A few cases with small q and $R_{\rm A}/R_0$ have kinetic angular momentum flux exceeding the magnetic angular momentum flux, but otherwise the solutions are magnetically dominated.

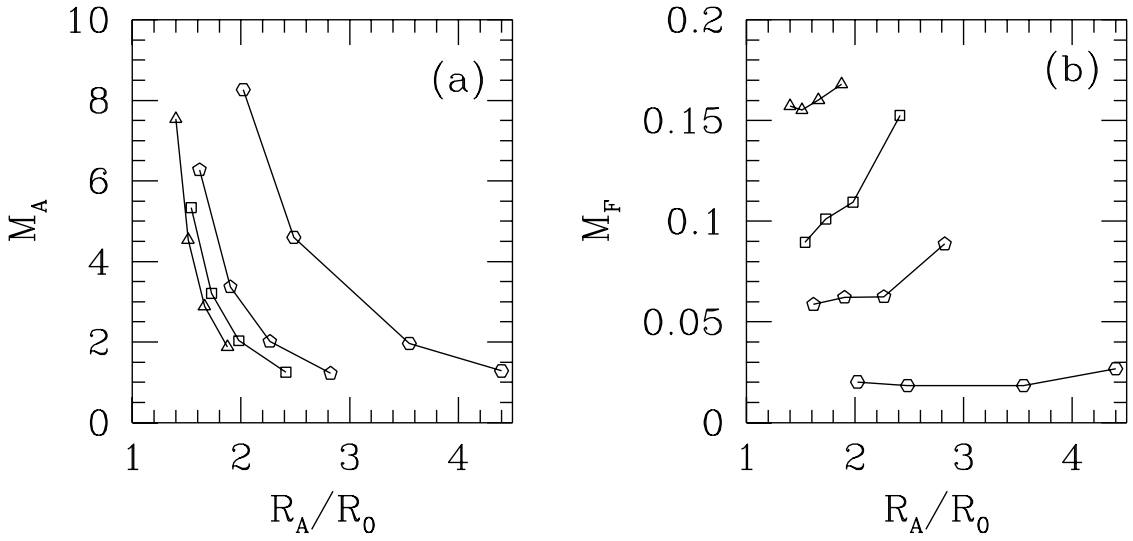

Fig. 5.— Asymptotic Alfvén and fast MHD Mach numbers $M_{\rm A} \equiv v_{\rm p}/v_{\rm A,p}$ (a) and $M_{\rm F} \equiv v_{\rm p}/v_{\rm A}$ (b) for r-similar solutions with various parameters. Triangles show solutions with $q = 0.5$; squares $q = 0.75$; pentagons $q = 0.9$; hexagons $q = 0.99$. Solid lines connect the solution points.

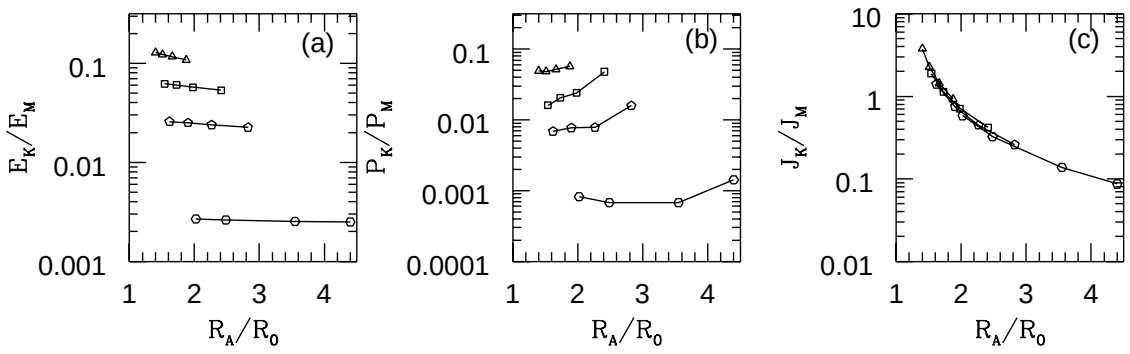

Fig. 6.— Asymptotic ratios of kinetic to magnetic energy flux (a), momentum flux (b), and angular momentum flux (c) for r-similar solutions with various parameters. Triangles show solutions with $q = 0.5$; squares $q = 0.75$; pentagons $q = 0.9$; hexagons $q = 0.99$. Solid lines connect the solution points. See text for definitions of fluxes.

4. Summary and Discussion

The calculations presented in this paper explore the proposal that observed narrow optical jets from PMS stars faithfully represent an inherent strong collimation in both density and velocity of the winds which are magnetocentrifugally driven from these young star/disk systems. To this end, we have developed models of MHD disk winds in which all streamlines asymptote to lie on the surfaces of a series of nested cylinders, at large distances from the disk. To make these calculations tractable, we work within the framework of radially self-similar flows, for which the density ρ, all magnetic field strengths B, and all velocities v have power-law scaling in the spherical radius r: $\rho \propto r^{-q}$, $B \propto r^{-(1+q)/2}$, and $v \propto r^{-1/2}$, for arbitrary q. The shape of wind streamlines and the dependence of all flow quantities on θ are then calculated self-consistently from the steady-state MHD equations. The r-self-similar ansatz is a convenient mathematical idealization, and also may serve as a good characterization of the possible flows well away from the boundaries of a disk with large dynamic range. Along a ray of $\theta = const.$, the decrease of the dynamical variables ($\mathbf{v}$, $\mathbf{B}$, ρ) with r occurs because the collimation of the flow brings streamlines from successively more distant regions of the disk to cross the ray. Since the farther regions of the disk are characterized by lower velocity, and by assumption lower density ρ and magnetic field strength B, the wind will reflect these decreases correspondingly. Note in particular that the present mathematical formalism allows for fast flows at large distance r from the source even though $v \propto r^{-1/2}$: if v_p increases rapidly with decreasing θ (toward the $\hat{z}$-axis), then a "jetlike" flow can exist along the pole.

We begin our analysis, in §2.2, by presenting an exact, analytic family of solutions for rotating, cylindrically-symmetric, axial ($v_R, B_R = 0$) MHD flows which are self-confined by gradients in the toroidal magnetic field. All flow variables are independent of the distance along the flow axis z, and have power-law dependence $\rho \propto R^{-q}$, $B_\varphi \propto B_z \propto R^{-(1+q)/2}$, $v_\varphi \propto v_z \propto R^{-1/2}$ on the cylindrical radius $R = r \sin\theta$. The three-parameter family of solutions can be described by q together with j and e, where the latter two respectively are the specific angular momentum, and the Bernoulli constant (equivalent to the fluid energy in a rotating frame), in units of local rotation rate of a magnetic field line Ω and cylindrical radius R. These parameters are natural to use when connecting to a flow from a disk in Keplerian rotation. This fully-analytic family of shearing, rotating, axial winds includes both sub- and super- fast MHD flows, i.e. $v_z <$ or $> v_{\rm A}$. The presence of a toroidal field $v_{{\rm A},\varphi} \neq 0$ permits confinement of rotating flows in which the magnetic pressure decreases to larger R – i.e., flows in which the outward centrifugal force and outward pressure gradient forces are balanced by an inward magnetic tension ("hoop stress"). In order for this to work, however, the gradient in the magnetic field cannot be too steep: for self-similar flows, cylindrical collimation is only possible if B drops with R no faster than R^{-1}, i.e. $q < 1$.

We next, in §3, take the family of rotating, shearing cylindrical flows as the set of desired asymptotic boundary conditions far from the disk, and ask what sort of magnetocentrifugally-driven disk winds can achieve this fully collimated state. We present a range of solutions for various q, $e = (3/2)(R_0/R_1)^2$ and $j = (R_{\rm A}/R_1)^2$, where R_0 is the position of a streamline's footpoint in the disk, $R_{\rm A}$ is the Alfvén radius, and R_1 is the asymptotic radius. Note that the self-similarity of the flow makes e and j the same for all streamlines. For each q and e there is a unique j for which the flow passes smoothly through the Alfvén point; thus the family of r-similar disk winds which become cylindrically collimated is labeled by two parameters. The asymptotic characteristics shared by all the self-collimating wind solutions presented are (1) $v_z/\Omega R_0 \sim$ few $\times 0.1$, (2) $v_\varphi/\Omega R_0 \sim$ few - several $\times 0.1$, (3) $v_{{\rm A},\varphi}/v_{\rm A,p} >> 1$, and (4) $v_z/v_{\rm A} < 1$. Here, Ω is the Kepler speed in the disk at the streamline's footpoint R_0. In particular, note that unlike in most previous MHD disk wind solutions (which, however, have unconstrained asymptotic states), these flows do not accelerate to final axial speeds comparable to or larger than the escape speed from the potential well where they originated. Thus, for example, if the innermost streamline originates near the surface of a PMS solar-type star, then based on the present solutions the maximum outflow speed along the central axis of the "jet" would only be a few to several tens of $\mathrm{km\,s^{-1}}$, much lower than the optical Herbig-Haro jets observed to reach a few hundred $\mathrm{km\,s^{-1}}$ speeds. Intuitively, the result (4) may be understood as follows: a cold MHD flow must leave the disk at an angle at least 30° from the vertical. In order to be fully redirected upwards, $v_{{\rm A},\varphi}$ must be $\gtrsim v_{\rm p}$ to accomplish the refocusing. But after the flow has been redirected, it is left in sub-fast-MHD state.

Because the fully-collimated disk wind solutions we have found have relatively low final speeds, we believe that observed optical jets from YSOs are unlikely to be manifestations of these or similar flows. Among the many possible alternative models, we list a few:

(1) The wind responsible for the observed jet originates in the disk, and its final velocity collimation is large but less extreme than the present solutions. Contopoulos & Lovelace (1994) have identified solutions with q slightly greater than one which continue expanding laterally (in R) up to the limit of their integration in z, and have $v_{\rm p}/\Omega R_0 > 1$. It would be interesting to compare the density and momentum distributions in such solutions with observed jets.

(2) A well-collimated MHD disk wind like those computed in this paper comprises an unseen neutral wind which surrounds the optical jet and enforces its observed collimation; the wind would also help drive outflows by directly sweeping up ambient material far from the jet. The jet itself must originate inside of the collimating wind, and have a more efficient acceleration mechanism (perhaps involving relatively strong poloidal magnetic

fields to achieve the magnetic "propeller" effect). Since in this case the jet is not required to self-collimate its velocity vectors, the flow which produces the jet could emerge from near the star in a relatively isotropic fashion.

(3) As in the model of Shu et al (1994a,b), Najita & Shu (1994), and Shu et al (1995), the whole of the wind originates in a narrow region of the disk near the star and flows outward with nearly radial poloidal streamlines and speeds comparable to the stellar escape speed for the whole flow. At large distances from the star, the velocity field is still nearly radial with only logarithmic streamline collimation due to toroidal field stresses. In this case, however, the density appears much more cylindrically collimated than the velocity field, and the optical jet may represent just the densest part of the wind near the axis.

Since the models presented herein are not "global" in the sense of physically matching to interior and especially exterior ambient conditions, it is more difficult to assess the possible relationship between such winds and observed molecular outflows. A real disk has a real inner and outer edge, and thus there must be a first and last wind streamline. If we arbitrarily truncate the source of the self-similar wind at the inside and outside disk edges $R_0 = R_*$ and $R_0 = R_{\rm D}$, then the first and last streamlines would exit the disk at a finite angle[2] and asymptote to helically wrap around the surfaces of cylinders of inner and outer radii $R_{\rm C} = (R_1/R_0)R_*$ and $R_{\rm W} = (R_1/R_0)R_{\rm D}$, respectively. If we assume a central star of mass $M_\star$ and total mass-loss rate $\dot{M}_{\rm W}$ in the wind between R_* and $R_{\rm D}$, then we can introduce dimensional scales for the density, magnetic field, and velocity to write the asymptotic profile in the wind at cylindrical distance R from the axis as

$$\rho = \rho_{\rm W} \left(\frac{R}{R_{\rm W}}\right)^{-q}, \tag{44}$$

$$\mathbf{B} = \mathbf{B}_{\rm W} \left(\frac{R}{R_{\rm W}}\right)^{-(1+q)/2}, \tag{45}$$

and

$$\mathbf{v} = \mathbf{v}_{\rm W} \left(\frac{R}{R_{\rm W}}\right)^{-(1/2)}. \tag{46}$$

Here,

$$\rho_{\rm W} = 4.5 \times 10^5 \ {\rm cm}^{-3} \mu_H \left(\frac{\dot{M}_{\rm W}}{10^{-7} {\rm M}_\odot \ {\rm yr}^{-1}}\right) \left(\frac{M_\star}{{\rm M}_\odot}\right)^{-1/2} \left(\frac{R_{\rm D}}{100 \ {\rm AU}}\right)^{-3/2} \left(\frac{R_0}{R_1}\right)^2 \left(\frac{v_z}{\Omega R_0}\right)^{-1} N_q \tag{47}$$

[2]Note that to maintain force balance near the outer disk edge there would in fact need to be additional wind streamlines filling the region toward the equatorial plane.

is the density on the outermost wind streamline,

$$\mathbf{B}_{\rm W} = \left(\frac{v_{{\rm A},z}}{\Omega R_0}, \frac{v_{{\rm A},\varphi}}{\Omega R_0}\right) \times 0.92{\rm mG}\left(\frac{\dot{M}_{\rm W}}{10^{-7}{\rm M}_\odot\ {\rm yr}^{-1}}\right)^{1/2}\left(\frac{M_\star}{{\rm M}_\odot}\right)^{1/4}\left(\frac{R_{\rm D}}{100\ {\rm AU}}\right)^{-5/4}\left(\frac{R_0}{R_1}\right)\left(\frac{v_z}{\Omega R_0}\right)^{-1/2} N_q^{1/2} \quad (48)$$

gives the magnetic field components on the outermost streamline, and

$$\mathbf{v}_{\rm W} = \left(\frac{v_z}{\Omega R_0}, \frac{v_\varphi}{\Omega R_0}\right) \times 3.0\ {\rm km\,s^{-1}}\left(\frac{M_\star}{{\rm M}_\odot}\right)^{1/2}\left(\frac{R_{\rm D}}{100\ {\rm AU}}\right)^{-1/2} \quad (49)$$

gives the components of the wind velocity on the outermost streamline;

$$N_q \equiv \frac{3/2 - q}{1 - (R_*/R_{\rm D})^{3/2-q}} \quad (50)$$

is a normalization constant. The values of R_0/R_1, and asymptotic $v_z/\Omega R_0$, $v_\varphi/\Omega R_0$, $v_{{\rm A},z}/\Omega R_0$, and $v_{{\rm A},\varphi}/\Omega R_0$ are shown for various models in figures 3d and 4a-d of §3.

The pressure in the wind is dominated by $B_\varphi^2/8\pi$. While the very innermost part of the parent cloud core may have comparable pressure (at density $\sim 10^8$ cm^{-3}), the outer cloud core ambient medium will generally have pressure far below that of the wind. Thus, either the wind as a whole or its surface layers would have to expand laterally until the pressure matches the ambient medium (which event occurs depends in part on the stability of the wind, a question under current investigation).

If the wind expands as a whole, keeping the mass load and poloidal speed on streamlines unchanged, then in the limit of negligible ambient pressure the wind would fill all 4π steradians. The far-asymptotic solution can be computed similarly to the calculation outlined in Shu et al (1995), if we assume that the flow streamlines adjust their latitudes θ at each r so that the force associated with the hoop stress (i.e. the gradient in $(RB_\varphi)^2$) is zero. The resulting streamlines and density contours have qualitatively similar behavior to the Shu et al (1995) results for a wind originating from a narrow region in the disk near the star. In particular, the distribution of wind momentum flux with angle has $d\dot{P}/d\cos\theta \sim C(r)R_0^{(1-q)/2}/(\sin\theta)^2$ for $C(r)$ a slowly-varying function, and R_0 the footpoint radius of the streamline that passes through θ at that r. For q near unity, this is nearly the same momentum distribution as that used by Li & Shu (1996) in their calculations of the lobe shapes and line profiles for swept-up molecular shells, so their results would carry over to the case of "fully expanded" disk winds. As Li & Shu (1996) showed, a momentum distribution near $d\dot{P}/d\cos\theta \propto 1/(\sin\theta)^2$ and toroidal mass distribution $\rho_{\rm amb} \propto \sin^2\theta$ in the ambient medium well reproduces the parabolic outflow shell shapes and line profile wings

$dM_{sh}/dv_{sh} \propto v_{\rm sh}^{-1.8}$ characteristic of many observed outflows. The coincidence in momentum distribution between the present case and the X-wind models occurs because here, the lower poloidal speeds on the outer disk streamlines are offset by a relatively greater mass load, compared to the X-wind models. Because winds from the outer portions of disks would have lower speeds but higher densities than the corresponding X-wind with the same momentum flux, the two cases could potentially be distinguished by the emission properties of the region where the wind impacts the ambient cloud. For example, finding H_2 emission at low latitudes in outflow shells would argue against disk-wind models for sweeping up the shell, because a shocked low-speed wind would not reach the few-thousand Kelvin temperature required.

If instead of the wind expanding as a whole, we assume that only the surface layers expand to match the pressure in the ambient medium, then much of the wind could retain its axial poloidal velocity field. The distribution of axial momentum flux in this interior portion would obey $d\dot{P}/dR \propto R^{-q}$. If this inner wind sweeps up a shell from a surrounding cloud core with initial density distribution $\rho_{\rm amb} \propto z^{-a}$, then the distribution of mass with velocity v_s in the shell would obey $dM_{sh}/dv_{sh} \propto v_{sh}^{-4/(1+q)+a(1-q)/(1+q)}$. For q near unity, or a near 2 (as for the Shu (1977) singular isothermal sphere), the power in the distribution is near -2, in good agreement with the -1.8 dependence cited by Masson & Chernin (1992) for the high-velocity part of observed outflow line profiles. Without a model for how the wind on the outer streamlines expands and interacts with the ambient gas, however, it is impossible to tell whether such a "partially expanded" collimated disk wind would be consistent with observed outflow shapes and the distribution of low-velocity gas.

In summary, we believe that highly-collimated fast flows as defined by such famous jets as HH30, HH34, or HH111 are unlikely to represent the whole story of the primary winds from PMS star/disk systems. The models of this paper, though by no means an exhaustive survey of jet production possibilities, show that it may be difficult to generate strong *velocity* collimation and fast outflow self-consistently in a magnetocentrifugally-launched wind from an extended region of an accretion disk. The narrow appearance of fast optical jets from young stars therefore argues in favor of a surrounding wind, either from the whole of the disk or from near the star, which sustains the observed jet collimation and helps to drive molecular outflows on large scales.

This work was supported in part by a postdoctoral fellowship from the Harvard-Smithsonian Center for Astrophysics. It is a pleasure to acknowledge numerous discussions with Ramesh Narayan, Charles Gammie, and Jim Stone, as well as helpful comments on the manuscript from Bruce Draine and an anonymous referee.

A. Appendix

A.1. The Grad-Shafranov equation for r-self-similar flows

The Grad-Shafranov (GS) equation describes force balance in the direction perpendicular to the poloidal field lines. With the adoption of a radially self-similar form for the flow (eqs. 29 - 33), the GS equation becomes a second-order ODE for the reduced flux function $\phi(\theta)$. Denoting derivatives with respect to θ as primes, this equation can be written

$$\phi'' = \frac{\mathcal{R}}{\mathcal{L}} \tag{A1}$$

where

$$\begin{aligned}\mathcal{L} &= (mnb^2-1)\left\{mnb^2\left[2\left(\frac{R_0}{R_1}\right)^3\sin\theta+\omega^2-2e\epsilon\right]-h\left(\frac{\phi\sin\theta}{nb}\right)^2\right\} \\ &= \left[\left(\frac{v_{\rm A,p}}{v_{\rm p}}\right)^2-1\right]\left(\frac{R_0}{R_1}\right)^3\frac{(v_{\rm A}^2-v_\theta^2)}{GM/R}\end{aligned} \tag{A2}$$

and $\mathcal{R} = \mathcal{R}_1 + \mathcal{R}_2 + \mathcal{R}_3$. Here,

$$\begin{aligned}\mathcal{R}_1 = \frac{3-q}{4}\frac{\mathcal{D}(bn)^2}{\phi h\sin^2\theta}\times \\ \left\{(q+1)mnb^2\left[2\left(\frac{R_0}{R_1}\right)^3\sin\theta+\omega^2-2e\epsilon\right]-2\left(\frac{R_0}{R_1}\right)^3\sin\theta+2\frac{(j\ell)^2-mnb^2\omega^2}{1-mnb^2}\right\},\end{aligned} \tag{A3}$$

$$\mathcal{R}_2 = \mathcal{D}(1-mnb^2)\phi'\left(3\frac{\cos\theta}{\sin\theta}+\frac{q+1}{3-q}\frac{\phi'}{\phi}\right) \tag{A4}$$

and

$$\begin{aligned}\mathcal{R}_3 = (1-mnb^2)\left(\phi'+\frac{3-q}{2}\frac{\cos\theta}{\sin\theta}\phi\right)\times \\ \left\{\frac{h}{2(nb)^2}\left[\left(\frac{2}{3-q}\right)^2\frac{\phi'}{\phi}\sin\theta\left(5\phi\cos\theta+\frac{2q}{3-q}\phi'\sin\theta\right)\left(\phi'+\frac{3-q}{2}\frac{\cos\theta}{\sin\theta}\phi\right)+\frac{2}{3-q}\phi'\phi\right]\right. \\ \left.-\left(\frac{R_0}{R_1}\right)^3\cos\theta-\frac{2e\epsilon-3\omega^2}{3-q}\frac{\phi'}{\phi}+\frac{(j\ell-\omega)(j\ell+3\omega)}{(3-q)(1-mnb^2)^2}\frac{\phi'}{\phi}\right\},\end{aligned} \tag{A5}$$

with

$$\mathcal{D} = mnb^2\left[2\left(\frac{R_0}{R_1}\right)^3\sin\theta+\omega^2-2e\epsilon\right]-\frac{hQ^2}{(nb)^2}$$

$$= (mnb^2 - 1)\left[2\left(\frac{R_0}{R_1}\right)^3 \sin\theta + \omega^2 - 2e\epsilon\right] + \frac{(j\ell - \omega)^2}{(1 - mnb^2)^2}$$
$$= \left(\frac{R_0}{R_1}\right)^3 \frac{(v_{\rm A}^2 - v_{\rm p}^2)}{GM/R}. \tag{A6}$$

The function Q, which is proportional to the poloidal field strength, is defined in equation (40). The constants e, j, m, and h are defined in §2.3. The first two are the free parameters which must be chosen before initiating an integration, while m and h may be expressed in terms of e and j using the asymptotic cylindrical solution (see eqs. 24 and 37).

A.2. Asymptotic boundary conditions

The equation (A1) contains terms that scale as $(\sin\theta)^{-2}$ and $(\sin\theta)^{-1}$, and this singular behavior near the pole demands special treatment. The method is to approximate

$$\phi(\theta) = 1 + \phi'(0)\theta + \phi''(0)\theta^2/2 \tag{A7}$$

near the pole, and then to expand the governing equation (A1) in θ and collect terms at each order. The only part of equation (A1) that contains terms of order $(\sin\theta)^{-2}$ is $\mathcal{R}_1$, and equation (23) shows that the expression in curly braces in equation (A3) contains no order-unity terms. This verifies that the cylindrical solution presented in §2.2 is a valid limiting solution of the full self-similar wind equations, to lowest asymptotic order. Next, we must collect the order $(\sin\theta)^{-1}$ terms in the expansion of equation (A1). By requiring that the corresponding coefficient be zero, after some algebra we obtain a linear equation which we solve for $\phi'(0)$ in terms of q, e, and j. Finally, the expansion of (A1) to order 1 is linear in $\phi''(0)$; rather than performing the expansion analytically, however, we numerically solve for the value of $\phi''(0)$, once q, e, j, and $\phi'(0)$ are set. After solving for $\phi''(0)$, we choose a value for θ_1 (typically 10^{-4} is adequate) at which to initiate the integration, then evaluate ϕ at θ_1 via equation (A7), set $\phi'(\theta_1) = \phi'(0) + \phi''(0)\theta_1$, and begin the numerical integration.

A.3. Alfvén transition constraints

As discussed by BP and other authors, equation (A1) can become singular if $\mathcal{L} = 0$, which from equation (A2) occurs if $v_{\rm A,p} = v_{\rm p}$ (i. e. $M_{\rm A} = 1$) or $v_{\rm A} = v_\theta$. For waves propagating along the $\hat{\theta}$ direction (i.e. along the spatial direction corresponding to the only degree of freedom for a radially self-similar flow), the first case corresponds to an Alfvén transition in v_θ, and the second case to a fast MHD transition in v_θ. To avoid singularities,

physical solutions must have $\mathcal{R} = 0$ wherever $\mathcal{L} = 0$; such points become critical points of the flow, and the requirement that the flow passes smoothly through these critical points constrains the possible values of the parameters entering the solution. It turns out that for the solutions presented in this work, $|v_\theta| < v_{\rm A}$ throughout the flow, so there is no fast MHD critical point. The Alfvén critical point, however, does impose constraints on the possible values of the parameters j and e.

At the Alfvén point where $M_{\rm A} = 1$, we use the streamline-invariant equations (38) to evaluate ω, b, ℓ, and ϵ in terms of $\phi(\theta_{\rm A}) \equiv \phi_{\rm A}$. Then, from equation (12), a smooth solution requires $j\ell - \omega|_{\rm A} = 0$ so that $\phi_{\rm A} = j^{-(3-q)/4}$ must obtain. Using the definition $M_{\rm A}^{-2} = mnb^2$, the reduced density at the Alfvén point must be given by $n_{\rm A} = j^{q/2}/m$. The Bernoulli equation at the Alfvén point becomes

$$\left.\frac{d(M_{\rm A}^{-2})}{d\theta}\right|_{\rm A} = \left.\frac{4\omega\phi'}{(3-q)\phi\mathcal{D}^{1/2}}\right|_{\rm A}, \tag{A8}$$

where $\mathcal{D}$ is defined in equation (A6). Finally, the Bernoulli and GS equations at the Alfvén point can be combined to yield the requirement that $\phi'_{\rm A}$ must be a solution of

$$1 = \left.\frac{(4\omega)^2\left[\omega^2 - 2e\epsilon + 2\left(\frac{R_0}{R_1}\right)^3\sin\theta - \frac{h\phi}{(nb)^2}\left(\phi + \frac{2\phi'\sin\theta\cos\theta}{3-q}\right)\right]^2}{\mathcal{D}\left\{q\left[\omega^2 - 2e\epsilon + 2\left(\frac{R_0}{R_1}\right)^3\sin\theta\right] + 3\omega^2 - 2e\epsilon\right\}^2}\right|_{\rm A}. \tag{A9}$$

Thus, the values at the Alfvén point of ϕ, ω, b, ℓ, ϵ and n are determined from the initial conditions at the pole, while the required value of $\phi'_{\rm A}$ is given implicitly through equation (A9) in terms of these known parameters and the unknown position of the Alfvén point $\theta_{\rm A}$. For arbitrary values of the input parameters e and j, however, ϕ' at the point $\theta_{\rm A}$ where $\phi = \phi_{\rm A}$ will not satisfy equation (A9). Thus, one of the input parameters becomes an eigenvalue which is determined by the condition that equation (A9) is indeed satisfied, so that the solution is regular at the Alfvén point. We evaluate the eigenvalue using the shooting method. Specifically, we choose values of q and R_0/R_1 (i.e. $e = (3/2)(R_0/R_1)^2$), and guess a value of $R_{\rm A}/R_1$ (i.e. $j = (R_{\rm A}/R_1)^2$). We then numerically integrate from the pole up to the Alfvén point, defined by the criterion $\phi = \phi_{\rm A}$. We use the error in equation (A9) near the Alfvén point to correct the guess for $R_{\rm A}/R_1$, and repeat until a satisfactorily converged solution is obtained for the super-Alfvénic region (typical error is $\sim 10^{-6} - 10^{-4}$ at the Alfvén point). We can then step over the Alfvén point, and continue the integration on the sub-Alfvénic side.

A.4. Equatorial boundary conditions

For integrations which start at the equator ($\theta = \pi/2$), divergence of $n(\theta)$ (since $v_{\rm p} \to 0$ in the cold-flow limit) means we must analytically expand the relevant equations in $\delta = \pi/2 - \theta$. For a given value of R_0/R_1 (i.e. e), we have $\phi(\pi/2) \equiv \phi_e = (R_0/R_1)^{-\frac{3-q}{2}}$ from equation (29), and from equation (38) we obtain the equatorial values of the other streamline invariants. Given an arbitrary value for $\phi'(\pi/2) \equiv \phi'_e$, the lowest-order expansion of the Bernoulli equation (39) yields the approximation for the reduced density function

$$n(\delta) = (mb_e^2\delta)^{-1}\left\{hm^2\left(\frac{R_0}{R_1}\right)^{-6}\left[1+\left(\frac{2}{3-q}\right)^2\left(\frac{\phi'_e}{\phi_e}\right)^2\right]+\left[\left(\frac{R_{\rm A}}{R_0}\right)^2-1\right]^2\right\}^{1/2}\times \left[-1+3\left(\frac{2}{3-q}\right)^2\left(\frac{\phi'_e}{\phi_e}\right)^2\right]^{-1/2}, \quad \text{(A10)}$$

where here and in the following the "e" subscript denotes evaluation at $\theta = \pi/2$. From this equation, it is clear that solutions require $(3-q)/(2\sqrt{3}) < |\phi'_e|/\phi_e$; this condition is equivalent to the well-known requirement that streamlines leave the disk at an angle $> 30^\circ$ with respect to the vertical (BP).

Next, given some choice for ϕ'_e, we can expand the Grad-Shafranov equation (A1) to lowest order in δ. The result is linear equation which yields ϕ''_e in terms of q, e, j, and ϕ'_e. For fixed q, we can identify a pair (j, e) which satisfies the requirements for a smooth transition at the Alfvén point when approached from the pole, as described in §A.3. We can then iteratively solve for the value of ϕ'_e which allows an equatorially-initiated sub-Alfvénic solution to match smoothly onto the pole-initiated super-Alfvénic solution at the Alfvén point. We generally proceed by choosing a value for R_0/R_1 and then searching for the unique values of $R_{\rm A}/R_1$ and ϕ'_e which yield a smooth match at the Alfvén point. When sufficiently accurate values are determined, the pole-initiated and equator-initiated solutions can generally cross the Alfvén point and overlap the solution on the far side, with very small errors.

REFERENCES

Bachiller, R. 1996, ARAA, 34, 111

Bachiller, R. & Gomez-Gonzalez, J. 1992 Astronomy and Astrophysics Review, 3, 257

Begelman, M. C., Blandford, R. D., & Rees, M. J. 1984, Rev. Mod. Phys., 56, 255

Blandford, R. D. 1990, in Active Galctic Nuclei, by R.D. Blanford, H. Netzer, & L. Woltjer (Berlin: Springer-Verlag), p. 161

Blandford, R. D. & Payne, D. G. 1982, MNRAS, 199, 883 (BP)

Blondin, J. M., Fryxell, B. A., & Königl, A. 1990, ApJ, 360, 370

Bogovalov, S. V. 1994, MNRAS, 270, 721

Bridle, A. H., & Perley, R. A. 1984, ARAA, 22, 319

Chernin, L. M., & Masson, C. R. 1995, ApJ, 455, 182

Chernin, L. M., Masson, C. R., Gouveia Dal Pino, E. M., & Benz, W. 1994, ApJ, 426, 204

Chiueh, T., Li, Z. -Y., & Begelman, M. C. 1991, ApJ, 377, 462

Contopoulos, J. 1994, ApJ, 432, 508

Contopoulos, J. 1995, ApJ, 450, 616

Contopoulos, J., & Lovelace, R. V. E. 1994, ApJ, 429, 139 (CL)

Edwards, S., Ray, T., & Mundt, R. 1993 in Protostars and Planets III, ed. E. Levy & J. Lunine (Tucson: Univ. of Arizona Press), p. 567

Ferriera, J. 1996, A&A, in press

Ferreira, J., & Pelletier, G. 1995, A&A, 295, 807

Fukui, Y., Iwata, T., Mizuno, A., Bally, J., & Lane, A. P. 1993, in Protostars and Planets III, ed. E. Levy & J. Lunine (Tucson: Univ. of Arizona Press), p. 603

Hartigan, P., in Accretion Phenomena and Related Outflows, ed. G. Bicknell, L. Ferrario, & D. Wickramasinghe, in press

Hartigan, P., Edwards, S., & Ghandour, L. 1995, ApJ, 452, 736

Heathcote, S., Morse, J. A., Hartigan, P., Reipurth, B., Schwartz, R. D., Bally, J., & Stone, J. M. 1996, AJ, 112, 1141

Heinemann, M. & Olbert, S. 1978, JGR, 83, 2457

Heyvaerts, J. & Norman, C. 1989, ApJ, 347, 1055

Heyvaerts, J. & Norman, C. 1996, in Solar and Astrophysical Magnetohydrodynamic Flows, ed. K. C. Tsinganos (Dordrecht: Kluwer)

Koldoba, A. V., Ustyugova, G. V., Romanova, M. M., Chechetkin, V. M., & Lovelace, R. V. E. 1995, Ap&SS, 232, 241

Königl, A. 1989, ApJ, 342, 208

Königl, A., & Ruden, S. P. 1993, in Protostars and Planets III, ed. E. Levy & J. Lunine (Tucson: Univ. of Arizona Press), p. 641

Lada, C. J. 1985, ARAA, 23, 267

Lada, C. J., & Fich, M. 1996, ApJ, 459, 638

Li, Z.Y. 1995, ApJ, 444, 848

Li, Z.Y. 1996a, ApJ, 465, 855

Li, Z.Y. 1996b, ApJ, 473, 873

Li, Z. -Y., Chiueh, T., & Begelman, M. C. 1992, ApJ, 394, 459

Li, Z.Y., & Shu, F.H. 1996, ApJ, 472, 211

Livio, M. 1997, in Accretion Phenomena and Related Outflows, ed. G. Bicknell, L. Ferrario, & D. Wickramasinghe, in press

Masson, C. R., & Chernin, L. M. 1992, ApJ, 387, L47

Masson, C. R., & Chernin, L. M. 1993, ApJ, 414, 230

Nagar, N. M., Vogel, S. N., Stone, J. M., & Ostriker, E. C. 1997, ApJ(Letters), submitted

Najita, J. R., & Shu, F. H. 1994, ApJ, 429, 808

Norman, C., & Silk, J. 1980, ApJ, 238, 158

Ouyed, R., Pudritz, R. E., & Stone, J. M. 1996, Nature, 385, 409

Pringle, J. 1981, ARA&A, 19, 137

Pudritz, R. E., & Norman, C. A. 1986,ApJ, 301, 571

Raga, A., & Cabrit, S. 1993, A&A, 278, 267

Ray, T. P., Mundt, R., Dyson, J. E., Falle, S. A. E. G., Raga, A. C. 1996, ApJ, 468, L103

Rosso, F., & Pelletier, G. 1994, A&A, 287, 325

Reipurth, B., & Cernicharno, J. 1995, Rev. Mexicana Astron. Astrfis. (Serie de Conferencias), 1, 43

Sakurai, T. 1985, A&A, 152, 121

Sakurai, T. 1987, PASJ, 39, 821

Sauty, C. , & Tsinganos, K. 1994, A&A, 287, 893

Shibata, K., & Uchida, Y. 1986, PASJ, 38, 631

Shu, F. H. 1977, ApJ, 214, 488

Shu, F. H. 1996, in Molecular Clouds and Star Formation, ed. C. Yuan & J. You (World Scientific: Singapore), p. 97

Shu, F.H., Adams, F.C. & Lizano, S. 1987, ARA&A, 25, 23

Shu, F. H., Najita, J., Ostriker, E., Wilkin, F., Ruden, S. P., & Lizano, S. 1994, ApJ, 429, 781

Shu, F. H., Najita, J., Ruden, S. P., & Lizano, S. 1994, ApJ, 429, 797

Shu, F. H., Najita, J., Ostriker, E. C., & Shang, H. 1995, ApJ, 455, L155

Shu, F. H., Ruden, S. P., Lada, C. J., & Lizano, S. 1991, ApJ, 370, L31

Spruit, H. C. 1987, A&A, 184,173

Spruit, H. C. 1996, in Physical Processes in Binary Stars, eds. R. A. M. J. Wijers, M. B. Davies, & C. A. Tout (Dordrecht: Kluwer)

Stone, J. M., & Norman, M. L. 1993, ApJ, 413, 198

Stone, J. M., & Norman, M. L. 1994, ApJ, 433, 746

Trussoni, E., Sauty, C., & Tsinganos, K. 1996, in Solar and Astrophysical Magnetohydrodynamic Flows, ed. K. C. Tsinganos (Dordrecht: Kluwer), p. 383

Tsinganos, K., Sauty, C., Surlantzis, G., Trussoni, E., & Contopoulos J. 1996, in Solar and Astrophysical Magnetohydrodynamic Flows, ed. K. C. Tsinganos (Dordrecht: Kluwer), p.427

Uchida, Y., & Shibata, K. 1985, PASJ, 37, 515

Ustyugova, G. V., Koldoba, A. V., Romanova, M. M., Chechetkin, V. M., Lovelace, R. V. E. 1995, ApJ, 439, L39

Wardle, M., & Königl, A. 1993, ApJ, 410, 218